Diploma thesis

Photoconductive Atomic Force Microscopy and Kelvin Probe Force Microscopy Measurements of Organic Semiconductor Nanostructures

by
Astrid Wachauer

at the Institute of Physics
Montanuniversität Leoben, Austria

under supervision of
Ao. Univ. Prof. Dr. Christian Teichert
Dr. Markus Kratzer
Dr. Igor Beinik

refereed by
Ao. Univ. Prof. Dr. Christian Teichert

Leoben, June 2011

dedicated to my family

Eidesstattliche Erklärung

Ich erkläre an Eides statt, dass ich diese Arbeit selbständig verfasst, andere als die angegebenen Quellen und Hilfsmittel nicht benutzt und mich auch sonst keiner unerlaubten Hilfsmittel bedient habe.

I declare in lieu of oath, that I wrote this thesis and performed the associated research myself, using only literature cited in this volume.

Astrid Wachauer
Leoben, June 2011

Abstract

Organic semiconductors are of increasing importance for electronic and optoelectronic device applications. They are inexpensive and easy to process on large flexible areas. Organic semiconductors are already used in organic light emitting diodes (OLED), organic field effect transistors (OFET), and organic solar cells.

The electronic properties of thin layers of organic semiconductors are known to be morphology dependent. The heterogeneity of the films impacts their optical and electrical transport properties. The main focus of the present work is the investigation of the electronic and optoelectronic properties of organic solar cells on the nanometer scale by means of photoconductive atomic force microscopy (PC-AFM) and photoassisted Kelvin probe force microscopy (PA-KPFM). Both, PC-AFM and PA-KPFM techniques allow the simultaneous detection of the electrical and optoelectrical properties along with the topography.

Here, the correlation between the heterogeneity and efficiency of the light-to-electricity conversion for blends with varying ratios of AnE-PV_{stat} and 1-(3-methoxycarbonyl) propyl-1-phenyl[6,6]C_{61} (PCBM) have been investigated. The AnE-PV_{stat} : PCBM samples showed a photoresponse under illumination with white light (150 W halogen lamp) at room temperature which is also confirmed by local current-to-voltage characterization. It has been revealed that measurements under ambient conditions result in degradation of the electrical properties. The photoresponse was partially recovered by annealing of the samples in nitrogen flow at 100°C. In the current maps a higher conductivity of the matrix compared to the grains is observed. In some cases small grains of 100 nm – 150 nm diameter with strongly reduced conductivity can be found. Contact potential difference (CPD) maps measured with PA-KPFM in general revealed a smaller CPD under illumination. Additionally, a smaller CPD of the matrix can be found, which is consistent with the higher conductivity observed with PC-AFM.

Other systems under investigation were polyvinylidene fluoride (PVDF) - poly(3-methylthiophene) (P3MT) core-shell nanoparticles with poly(3-hexylthiophene-2,5-diyl) (P3HT) binder and P3HT : PCBM blends on PVDF. The photoresponse in these systems was observed at room temperature and did not exhibit any signs of degradation when measured under ambient conditions. However, the topography images recorded using PC-AFM appeared blurry due to the weak mechanical stability of the samples.

Further, PC-AFM was also applied to investigate the temperature dependence of the photocurrent in C_{60} thin films under different degrees of illumination in order to verify the so called Meyer-Neldel rule. As expected, an Arrhenius dependence on the temperature was observed on films with different morphologies. However, the influence of the illumination by a 150 W xenon lamp on the measured current density appeared below the detection limits, which is due to fast degradation of the C_{60} thin films under

ambient conditions. The amorphous film has a thickness of 280 nm and consists of particles with 50 nm – 200 nm in diameter. The polycrystalline film consists of crystallites with sizes up to 700 nm, which is in the same size range as the film thickness of about 800 nm. Current images of the polycrystalline C_{60} film revealed the existence of smaller crystallites of up to 200 nm size that were nonconductive, indicating bad electrical contact to adjacent grains.

Kurzfassung

Organische Halbleiter sind von zunehmender Bedeutung für elektronische und optoelektronische Bauteilanwendungen. Sie sind kostengünstig und leicht auf großen biegsamen Flächen verarbeitbar. Organische Halbleiter werden bereits in organischen Leuchtdioden (OLED), organischen Feldeffekt Transistoren (OFET) und organischen Solarzellen eingesetzt.

Es ist bekannt, dass die elektrischen Eigenschaften von dünnen Schichten organischer Halbleiter von der Morphologie abhängig sind. Die Heterogenität der Filme beeinflusst ihre optischen und elektrischen Transporteigenschaften. Der Hauptschwerpunkt der vorliegenden Arbeit ist die Untersuchung der elektronischen und optoelektronischen Eigenschaften organischer Solarzellen auf der Nanometerskala mit Hilfe von Photoleitfähigkeits-Rasterkraftmikroskopie (PC-AFM) und Photogestützter Rasterkelvinsondenmikroskopie (PA-KPFM). Sowohl PC-AFM, als auch PA-KPFM ermöglichen eine gleichzeitige Messung der elektrischen und optoelektrischen Eigenschaften zusammen mit der Topografie.

Hier wurde der Zusammenhang zwischen der Heterogenität und der Effizienz der Licht-zu-Strom Umwandlung verschiedener Gemische mit unterschiedlichen Verhältnissen von AnE-PV$_{stat}$ und 1-(3-methoxycarbonyl)propyl-1-phenyl[6,6]C_{61} (PCBM) untersucht. Die AnE-PV$_{stat}$: PCBM Proben zeigten eine Reaktion auf Beleuchtung mit weißem Licht (150 W Halogenlampe) bei Raumtemperatur, was ebenfalls mittels lokaler Strom-Spannungs-Kurven bestätigt wurde. Es wurde gezeigt, dass Messungen unter Umgebungsbedingungen eine Verschlechterung der elektrischen Eigenschaften verursachen. Die Photoleitfähigkeit wurde durch Aufheizen der Probe im Stickstofffluss auf 100°C teilweise wiederhergestellt. In den Strombildern kann eine höhere Leitfähigkeit der Matrix gegenüber den Körnern beobachtet werden. In einigen Fällen können kleine Körner von 100 nm - 150 nm Durchmesser mit stark reduzierter Leitfähigkeit gefunden werden. Kontaktpotenzialdifferenz (CPD)-Bilder gemessen mit PA-KPFM zeigten generell eine Abnahme der CPD unter Beleuchtung. Zusätzlich konnte eine geringere CPD der Matrix gefunden werden, was mit der erhöhten Leitfähigkeit, welche mittels PC-AFM beobachtet werden konnte, übereinstimmt.

Weitere untersuchte Systeme waren Polyvinylidenfluorid (PVDF) - Poly (3-Methylthiophen) (P3MT) Kern-Hülle Nanopartikel mit Poly(3-Hexylthiophen-2,5-diyl) (P3HT) Binder sowie P3HT : PCBM Gemische auf PVDF. Eine Reaktion auf die Beleuchtung konnte bei diesen Systemen bei Raumtemperatur beobachtet werden, und zeigte auch keinerlei Anzeichen von Abbau bei Messungen unter Umgebungsbedingungen. Allerdings erschienen die mit PC-AFM aufgenommenen Topografie Bilder wegen der geringen mechanischen Stabilität der Proben verschwommen.

Weiters wurde PC-AFM auch zur Untersuchung der Temperaturabhängigkeit des

Photostroms in dünnen C_{60} Filmen unter verschiedenen Beleuchtungsgraden angewendet, um die sogenannte Meyer-Neldel Regel zu bestätigen. Wie erwartet, wurde eine Arrhenius Abhängigkeit über die Temperatur auf Schichten mit verschiedenen Morphologien beobachtet. Jedoch liegt der Einfluss der Beleuchtung mit einer 150 W Xenon Lampe auf die gemessene Stromdichte unterhalb der Messgrenze, was an der schnellen Zersetzung der dünnen C_{60} Filme unter Umgebungsbedingungen liegt. Die amorphe Schicht hat eine Dicke von 280 nm und besteht aus Teilchen mit 50 nm bis 200 nm Durchmesser. Die kristalline Schicht besteht aus Kristalliten, die bis zu 700 nm groß sind, was in der selben Größenordnung liegt, wie die Schichtdicke mit ungefähr 800 nm. Strombilder der polykristallinen C_{60} Schicht zeigen die Existenz von kleineren Kristalliten mit bis zu 200 nm Größe, welche keine Leitfähigkeit aufwiesen, was auf schlechten elektrischen Kontakt zu benachbarten Körnern hinweist.

Acronyms

AFM	Atomic Force Microscopy
AnE-PV$_{stat}$	PPE-PPV with varying side chains of octyl and 2-ethylhexyl
AR	Asylum Research
C-AFM	Conductive Atomic Force Microscopy
CB	Conduction Band
CPD	Contact Potential Difference
E_A	Activation Energy
E_{MN}	Meyer-Neldel Energy
HOMO	Highest Occupied Molecular Orbital
HWE	Hot Wall Epitaxy
I-V curve	Current-to-Voltage curve
ITO	Indium Tin Oxide
KPFM	Kelvin Probe Force Microscopy
LED	Light Emitting Diode
LUMO	Lowest Unoccupied Molecular Orbital
MFM	Magnetic Force Microscopy
MNR	Meyer-Neldel rule
NREL	National Renewable Energy Lab
OFET	Organic Field Effect Transistor
OLED	Organic Light Emitting Diode
P3HT	Poly(3-Hexylthiophene-2,5-diyl)
P3MT	Poly(3-Methylthiophene)

PA-KPFM	Photoassisted Kelvin Probe Force Microscopy
PC-AFM	Photoconductive Atomic Force Microscopy
PCBM	1-(3-methoxycarbonyl)propyl-1-phenyl[6,6]C_{61}
PEDOT	Poly(3,4-Ethylenedioxythiophene)
PPE-PPV	Poly(*p*-Phenylene-Ethynylene)-*alt*-poly-(*p*-Phenylene-Vinylene)
PVDF	Polyvinylidene Fluoride
RMS	Root Mean Square
SEM	Scanning Electron Microscopy
SPM	Scanning Probe Microscopy
T_{MN}	Meyer-Neldel Temperature
TR	Torsional Resonance
UHV	Ultra-High Vacuum
VB	Valence Band

Contents

Abstract iv

Kurzfassung vi

Acronyms viii

1 Introduction 1

2 Fundamentals 3
- 2.1 Electronic Properties of Organic Semiconductors . . . 3
  - 2.1.1 Organic Solar Cells . . . 3
  - 2.1.2 Organic Semiconductors for Solar Cells . . . 4
  - 2.1.3 The Meyer-Neldel Rule . . . 5
- 2.2 Preparation Methods for Organic Semiconductors . . . 8
  - 2.2.1 Spin Coating . . . 8
  - 2.2.2 Hot Wall Epitaxy . . . 8
- 2.3 Atomic Force Microscopy . . . 9
  - 2.3.1 Surface morphology characterization by Atomic Force Microscopy 10
  - 2.3.2 Photoconductive Atomic Force Microscopy . . . 10
  - 2.3.3 Kelvin Probe Force Microscopy . . . 11

3 Experimental 13
- 3.1 Sample preparation . . . 13
  - 3.1.1 Spin Coating . . . 13
  - 3.1.2 Hot Wall Epitaxy . . . 13
  - 3.1.3 Core-Shell Nanoparticles . . . 13
- 3.2 Atomic Force Microscopy . . . 15
  - 3.2.1 Current Measurement . . . 15
  - 3.2.2 Illumination . . . 16
  - 3.2.3 Determination of Film Thickness . . . 16
  - 3.2.4 AFM-Probes . . . 17
  - 3.2.5 Heating Cell . . . 17

4 Results 19
- 4.1 Organic Solar Cells . . . 19
  - 4.1.1 AnE-PV_{stat} : PCBM . . . 19
  - 4.1.2 PVDF-P3MT/P3HT : PCBM . . . 29

4.2 The Meyer-Neldel Rule on C_{60} films 37

5 Conclusions and Outlook **46**

Acknowledgments **49**

List of Figures **50**

Bibliography **55**

1 Introduction

Within the last two decades, efforts have been made to find new materials for electronic devices. The materials have to become cheaper and more easily to process on a large scale. Therefore organic semiconductors are a very good choice, compared to inorganic semiconductors, which are either very expensive, or difficult to produce. Organic semiconductors are already used for organic light emitting diodes (OLED), organic field effect transistors (OFET) and in organic solar cells. Especially organic solar cells are very interesting, since nowadays alternative energy sources are highly demanded. The burning of fossil fuels like mineral oil, natural gas and coal cause air pollution and influence the earth climate significantly. Furthermore, accidents during the mining and transportation of oil can pollute large regions in the ocean. Also the prices of these energy carriers increase every year. Another energy source is nuclear power, but this bears a great risk. Accidents, which can happen, no matter how many precautions are taken, can pollute wide regions for decades and cause various sicknesses and even death for people living close to the damaged power plant.

Solar cells are a relatively clean way to produce energy by direct conversion of the sunlight into electrical energy. Unfortunately, inorganic solar cells are too expensive in their production to use them on a large scale. By using organic semiconductors, processing costs can be reduced significantly. Furthermore, due to easy processing techniques, like spin coating and printing, which usually do not require heating of the substrate, these materials can be deposited on various substrates, including plastic sheets. By deposition of organic thin film solar cells on such substrates, flexible solar cells can be produced. Processing techniques like spin coating can also be used to obtain rather large solar cells, which is not possible with the processing techniques for inorganic solar cells. Together with the relatively low price of these cells, the market for solar cells increases dramatically. Compared to inorganic solar cells, organic solar cells have a lower charge carrier mobility and have a shorter lifespan due to their instability under ambient conditions. Furthermore, they have a rather high band gap of about 2 eV [1], whereby only a smaller fraction of the solar spectrum can be utilized. On the other hand, organic semiconductors have rather strong absorption coefficients, which increases the efficiency of the solar cells again. Most of organic solar cells are used in small devices, and therefore do not need very high efficiencies. Even though organic solar cells superior to their inorganic counterparts with restrict to several issues, boosting their efficiency is an important task. To increase the solar cell performance, obtained knowledge about the electrical properties on the nanoscale is indispensable. Therefore, scanning probe microscopy (SPM) techniques with which topography and electrical properties can be measured simultaneously are most suited [2].

Here, several solar cell materials were analyzed with atomic force microscopy (AFM)

to obtain morphological and electrical information on the nanometer scale. In the commonly used macroscopic measurements on solar cell devices, only the efficiency of the whole device can be measured, integrated over the whole sample area. With AFM techniques, the properties can be studied in more detail and on a small region. Furthermore, the photo electronic properties can be compared from different morphologies in the blend. With this detailed information on the electronic properties, the blends for organic solar cells can be optimized more efficiently.

AFM is an efficient tool to resolve morphological features on a nanoscale. In addition, with its variant conductive atomic force microscopy (C-AFM) [3], which is operated in contact mode, simultaneous measuring of the current between the sample and a conductive tip, which results from an applied sample bias, is possible. With Kelvin probe force microscopy (KPFM) [4], which is operated in tapping mode, the contact potential difference (CPD) between the sample and the tip, together with the topography can be measured. In photoconductive atomic force microscopy (PC-AFM) [3] and photoassisted Kelvin probe force microscopy (PA-KPFM) [5] optoelectrical properties can be analyzed by additional illumination of the sample during the measurement.

These studies were performed in collaboration with Alberto M. Ramil and Valery N. Bliznyuk from the group of Prof. Niyazi S. Sariciftci, and Mujeeb Ullah from the group of Prof. Helmut Sitter at the Johannes Kepler University Linz.

2 Fundamentals

2.1 Electronic Properties of Organic Semiconductors

The insulating character of most organic solids is well known to everyone, since they are frequently used in technical applications, like insulation of electrical wires. In addition, a large number of organic semiconductors exist. Within the last decades, they have increased in importance for electronic and optoelectronic devices, e.g. OLEDs, OFETs and organic solar cells. Besides, there exist also organic solids with a high dark conductivity, a quasi metallic-conductivity [6] and superconducting properties [6].

Very pure organic solids consisting of molecules with conjugated π-electron systems are insulators even at high temperatures. However, these materials turn into semiconductors, when charge carriers are either introduced by high external electric fields, or produced via the internal photoeffect by irradiation with electromagnetic waves or electrons. These π-electron systems are formed by sp^2-hybridized carbon atoms. The electrons in the p_z-orbitals of the molecules form π-bonds with each other. These orbitals are delocalized and therefore have a high electronic polarizability [1]. Conjugated π-electron structures are typical for aromatic molecules like benzene.

The single molecules have sharp energy states. Especially important are the highest occupied molecular orbital (HOMO) and lowest unoccupied molecular orbital (LUMO). In a crystal these states of the single molecules turn into bands, comparable to the valence band (VB) and conduction band (CB) in inorganic semiconductors. Organic semiconductors have a relatively high band gap of around 2 eV [1], while for example silicon has a band gap of only 1.1 eV.

In organic crystals, charge carriers polarize the neighboring molecules and form negative polarons, in the case of electrons, or positive polarons, in the case of holes. These polarons increase the effective mass of the charge carriers and thus influence the charge carrier mobility, which is in organic semiconductors usually lower than in inorganic ones [6].

2.1.1 Organic Solar Cells

Solar cells transform light into electric current. Inorganic solar cells consist of a p-n junction and two electrodes to collect the produced charge carriers. The irradiating light produces an electron-hole pair in the semiconductor by lifting an electron from the VB to the CB. Due to the internal electric field, which is generated in the depletion region in the p-n junction, the electrons are drawn to the n-type semiconductor and are collected by the electrode placed on that side, and the holes are drawn to the

p-type semiconductor and are collected by the other electrode [7]. In organic solar cells, the irradiating light produces an exciton, which will be described in detail in the next section. These excitons are split into electrons and holes at the interfaces between a p-type and an n-type semiconductor [1]. Usually, the different polymers are mixed in a blend and not arranged in layers, as in inorganic solar cells. To separate the charge carriers and draw them to the appropriate electrode, electrodes with different work functions, e.g. indium tin oxide (ITO), which has a high work function, and a metal with a low work function, like aluminum or magnesium, are used. The difference in work function produces a potential between the electrodes, which helps to split the excitons and drags the electrons to the positive electrode, in this case the ITO, and the holes to the negative electrode, here the metal.

2.1.2 Organic Semiconductors for Solar Cells

In organic semiconductors for solar cell applications, light excites electrons from the HOMO into the LUMO and leaving holes in the HOMO. These two different charge carriers can stay together in a bound state called exciton [1]. The mobility and diffusion length of these excitons are rather small. This effect reduces the efficiency of organic solar cells and different designs have to be used, to keep the negative influence of this effect to a minimum. Nevertheless, the high absorption coefficients of organic solar cells compensate for the poor charge-carrier mobility.

To separate an exciton in a pure polymer into an electron and a hole – which is necessary to collect current from a photovoltaic device – high electric fields have to be applied. However, it has been discovered in polymer-fullerene blends that excitons can be split into electrons and holes more efficiently [8,9], because it is energetically favorable to transfer the electron of the exciton to the more electronegative fullerene (C_{60}) molecule. More generally, excitons are split into separate positive and negative charge carriers at interfaces between a p-type electron donating and an n-type electron accepting material. [1,10]

In the following paragraphs, the organic semiconductors studied in this thesis are described in detail. Their chemical structures are shown in Fig.2.1.

P3HT

Like most organic semiconductors, poly(3-hexylthiophene-2,5-diyl) (P3HT) (Fig.2.1.b) is a p-type semiconducting polymer with photo- and electroluminescent character. The photovoltaic effect of the blend is produced by the excitation of the electrons in the π_z-orbitals of P3HT [11]. Due to its side chain it is soluble in chlorobenzene [1].

P3MT

Poly(3-methylthiophene) (P3MT) (Fig.2.1.e) is similar to P3HT, with the same semiconducting properties. It is used as the exciton producing polymer in blends of organic

solar cells. Because of the shorter side group, P3MT is not soluble in organic solvents which makes its processing more difficult.

AnE-PV$_{stat}$

AnE-PV$_{stat}$ is a statistical copolymer with anthracene containing poly(*p*-phenylene-ethynylene)-*alt*-poly-(*p*-phenylene-vinylene) (PPE-PPV) and different C_8H_{17}-side chains of linear octyl or branched 2-ethylhexyl. The different types of AnE-PV, as illustrated in Fig.2.1.a, show different properties. AnE-PV$_{aa}$ is insoluble and has a well ordered layer structure due to its linear side chains. AnE-PV$_{ab}$ is soluble and shows better solar cell performance, but has a less ordered structure. The polymers AnE-PV$_{ba}$ and AnE-PV$_{bb}$ are amorphous and have only poor photovoltaic properties. The mixture of these four types, called AnE-PV$_{stat}$, with statistically distributed octyl and 2-ethylhexyl side chains along the backbone, shows an increased photovoltaic performance. This polymer is also p-type semiconducting and produces the excitons in the blend [12].

PVDF

Polyvinylidene fluoride (PVDF) (Fig.2.1.c) is a piezoelectric [13] and ferroelectric polymer with outstanding mechanical properties which can be used within a wide temperature range. It consists of 1,1-difluoroethene, which is an ethene molecule where two hydrogen atoms are substituted by fluorine atoms. It is not semiconducting but is expected to improve the properties in organic solar cells due to its polarity [14].

PCBM

1-(3-methoxycarbonyl)propyl-1-phenyl[6,6]C_{61} (PCBM) (Fig.2.1.d) is similar to C_{60} and has the same n-type semiconducting character. The additional side group makes the molecule soluble in chlorobenzene. Therefore, PCBM can be processed more easily than C_{60}, e.g. by spin coating and printing techniques [15]. Therefore, it is the preferred n-type semiconductor in modern organic solar cells. This molecule is formed by attaching an additional methylene group onto a C_{60} molecule via a bridging reaction, where a C-C double bound is broken and bridged by another atom. Furthermore, the methylene group gets substituted on one side with a phenyl ring (C_6H_5) and on the other side with an ester of butyric acid and methanol, forming the methyl butyrate ((CH_2)$_3$-COO-CH_3).

2.1.3 The Meyer-Neldel Rule

The Meyer-Neldel rule (MNR) [18] is an empiric rule, which links the activation energy and the pre-exponential factor of a thermally activated process. The MNR applies for many processes in nature, like diffusion and conduction in semiconductors. Especially in semiconductors with a huge disorder and a great amount of traps, like organic, glassy, amorphous and porous materials, the MNR can be observed.

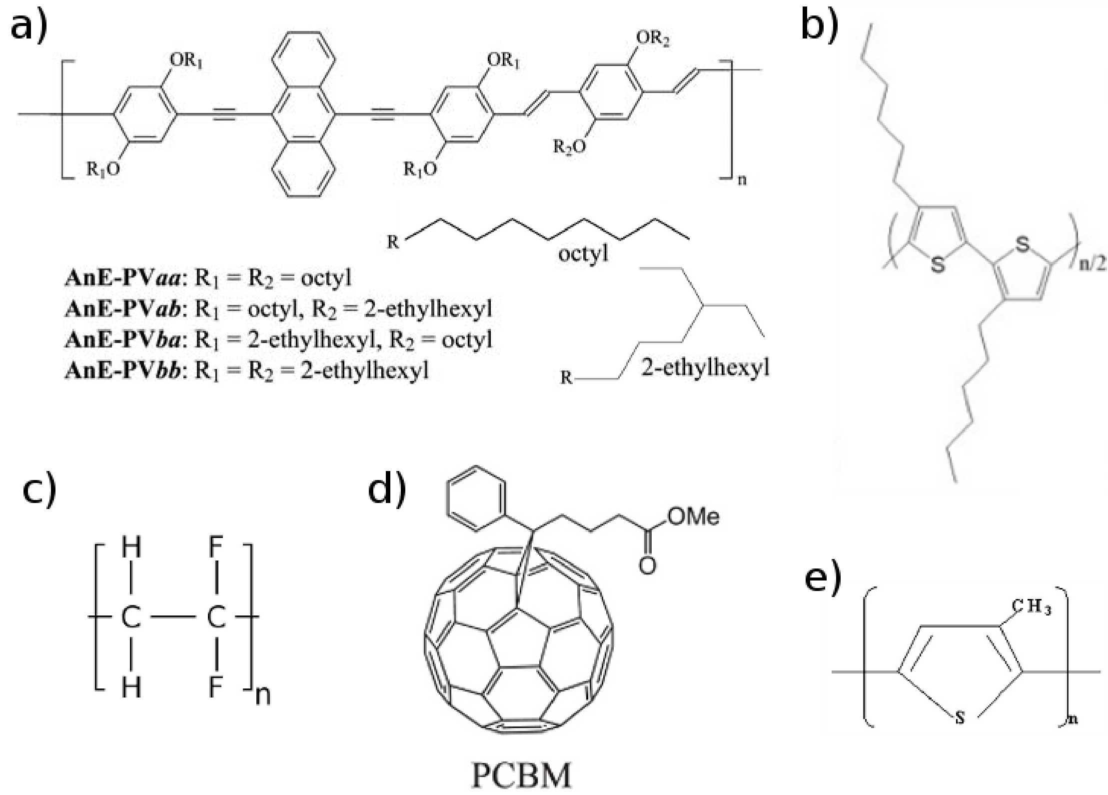

Figure 2.1: Chemical structures of the studied polymers: all types of AnE-PV and the different side chains octyl and 2-ethylhexyl [16] (a), P3HT [11] (b), PVDF (c), PCBM [11] (d) and P3MT [17] (e).

For the above mentioned materials the temperature dependence of the conductivity can be described via an Arrhenius function [19]:

$$\sigma = \sigma_0 \exp\left(\frac{-E_A}{k_b T}\right) \tag{2.1}$$

where σ is the conduction, σ_0 the pre-exponential factor, E_A the activation energy, here the band gap E_g, k_b the Boltzmann constant and T the absolute temperature.

The MNR states that the pre-exponential factor itself is dependent on the activation energy:

$$\sigma_0 = \sigma_{00} \exp\left(\frac{E_A}{E_{MN}}\right) \tag{2.2}$$

with σ_{00} as a constant factor and E_{MN} the so called Meyer-Neldel energy.

These formulas imply that the Arrhenius plots of the conductivity over the temperature for different activation energies, are straight lines with a single intersection point:

$$ln\sigma = ln\sigma_{00} + E_A \left(\frac{1}{E_{MN}} - \frac{1}{k_b T} \right) \tag{2.3}$$

This point is at an isokinetic temperature called the Meyer-Neldel temperature (T_{MN}), which is defined as T_{MN}=E_{MN}/k_b. Here, the multiplication term of E_A becomes zero, and the influence of the activation energy disappears. The MNR has been observed macroscopically in different materials for different electrical properties, e.g. the charge carrier mobility in C_{60} [20] and in pentacene [21]. Fig.2.2 shows the temperature dependence of the charge carrier mobility in OFETs with different applied gate voltages V_G, implying a variation of the of charge carrier concentration. The isokinetic temperature can be found at 250°C. [19–21]

The aim of our experiments was to observe the MNR also on the nanometer scale.

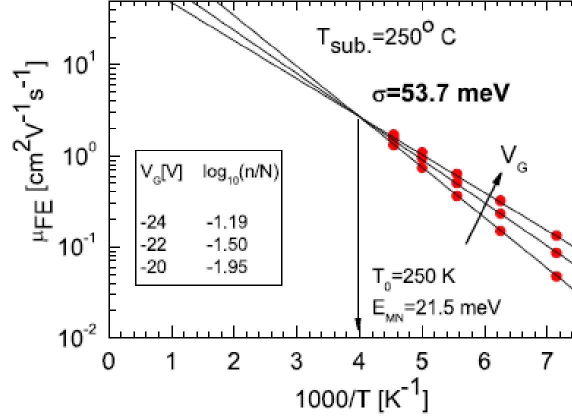

Figure 2.2: Macroscopic measurements of the field effect charge carrier mobility in a C_{60} OFET as function on temperature and charge carrier concentration modified via the applied gate voltage V_G (red points). The isokinetic temperature T_{MN}, here T_0, is indicated by an arrow. The C_{60} film was grown via hot wall epitaxy at 250°C substrate temperature. (From [20].)

2.2 Preparation Methods for Organic Semiconductors

For the processing of organic semiconductors two techniques are commonly used. Films of soluble polymers, which are larger due to their soluble side chains, are usually fabricated via wet processes, e.g. spin coating, drop casting and various printing techniques [15]. Therefore, the polymer is solved in a solvent and the solution is put onto the substrate by the techniques mentioned above. For small thermally stable polymers evaporation processes, e.g. hot wall epitaxy (HWE) and organic vapor phase deposition, are used [1].

2.2.1 Spin Coating

Spin coating is the most important deposition technique for solar cell devices nowadays, because very homogeneous films can be fabricated with high reproducibility. A liquid solution is applied to a spinning substrate and can be spread over a large area. The thickness and surface morphology depend on the rotation speed as well as on the viscosity, molecular weight, and concentration of the solute, whereas the deposited amount of solution is influencing the film parameters barely [15].

2.2.2 Hot Wall Epitaxy

HWE is the preferred growth method for Van der Waals epitaxy [22] of organic compounds, because films can be grown under conditions as close as possible to the thermodynamic equilibrium. Fig.2.3 shows the HWE-setup consisting of a quartz tube which acts as growth reactor and is filled with a small amount of source material. The tube is closed by the substrate in order to guarantee closed growth conditions and to reduce the loss of source material. The reactor has three separate ovens to adjust the temperatures of the different regions independently. One heater is at the bottom of the tube to vaporize the source material. The second heater is located between the source and the substrate, the so called hot wall. This region ensures an almost uniform and isotonic flux of molecules onto the substrate. The substrate can be heated with the third heater, as well as cooled with a Peltier element. In this way, the growth conditions can be tuned to get either crystalline or amorphous films. One main advantage of this growth method is that only high vacuum is necessary, while most other methods require ultra-high vacuum (UHV). Also the growth conditions can be varied in a wide range due to the separate heaters. A drawback is the bad reproducibility of the growth conditions and the missing in-situ control of the growth process. [22,23]

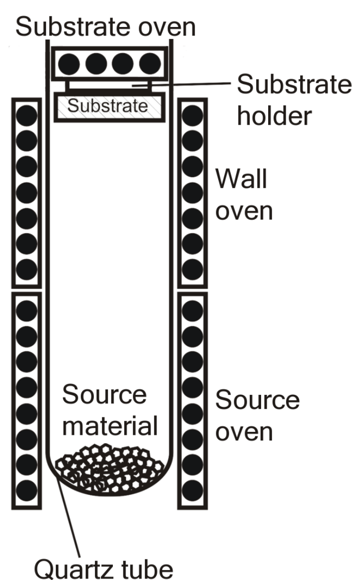

Figure 2.3: Schematic drawing of a HWE-setup.

2.3 Atomic Force Microscopy

Atomic force microscopy (AFM) is a SPM method which measures the interaction forces between the sample and a sharp tip, mounted on the free end of a cantilever. In contact mode, the tip is in permanent contact with the surface of the sample and the deflection of the cantilever is measured as function of the position. In tapping mode, the cantilever oscillates close to its resonance frequency and the damping of the amplitude by the interacting forces is determined. For measuring the movement of the cantilever, optical methods are commonly used. A light beam emitted by a laserdiode is focused on the cantilever and the position of the reflected beam is measured by a four-section split photodiode. A deflection of the cantilever results in a movement of the laser beam on the photodiode and changes the current between the different sections of the diode depending on the excentricity of the beam on the diode. With feedback configuration in contact mode, the deflection which corresponds to the resulting force on the tip, and in tapping mode the amplitude of oscillation is kept constant while the Z-piezo changes the distance between the sample and the probe. During scanning, the applied voltage on the Z-piezo is memorized as the surface topography. The X-Y scanning is done either by the same piezo scanner as the Z scanning, or by two additional piezo scanners. The lateral resolution of AFM is defined by the radius and the opening angle of the tip. On smooth surfaces, even atomic resolution can be achieved, especially in the so-called non-contact mode [2].

Besides morphology, one can probe physical properties on the nanometer scale by functionalyzing the tip, e.g. electrical properties with C-AFM and magnetic properties with magnetic force microscopy (MFM).

2.3.1 Surface morphology characterization by Atomic Force Microscopy

With AFM, the topography can be measured on the nanometer scale and analyzed with adequate software. The most important parameter to characterize the roughness of a surface is the root mean square (RMS)-roughness σ [24]. It describes the average height difference between the individual measurement points and the mean value of the height $\bar{z}$, and is defined as:

$$\sigma = \sqrt{\frac{1}{m \cdot n} \sum_{i=1}^{m} \sum_{j=1}^{n} (z_{ij} - \bar{z})^2} \tag{2.4}$$

where m and n are the number of points analyzed in x, respectively y direction, z_{ij} is the height at the point (i,j) and $\bar{z}$ the mean height of the analyzed area. The RMS-roughness increases for self-affine fractal surfaces with larger analyzed areas until a saturation is reached and the RMS roughness is constant.

Furthermore, the lateral correlation length ξ describes the lateral size of the morphological features and the roughness parameter α, also called Hurst parameter, characterizes the jaggedness of the surface roughness.

2.3.2 Photoconductive Atomic Force Microscopy

Photoconductive atomic force microscopy (PC-AFM) is a variant of C-AFM including additional illumination of the sample to analyze the photoelectric properties [3]. A schematic drawing of the setup is shown in Fig.2.4. C-AFM is an AFM operation in contact mode using a conductive cantilever and tip. An external voltage is applied between the tip and the sample and the resulting current is measured. Usually an external bias in the range of maximum ± 10 V is applied to the sample. The current measurement is independent from the simultaneously measured topography. The current signal has to be amplified and converted into a voltage signal before it is recorded by the software. The tip can also be positioned at a single spot to measure a local current-to-voltage curve (I-V curve) by ramping the applied bias and measuring the resulting current. In PC-AFM, the current can be measured as a function of illumination intensity and wavelength. By using the conductive probe as top contact, a nanoscale solar cell can be formed to measure the local photocurrent. There are several ways to illuminate the sample [3]. Illumination from the bottom ensures a better focus and a higher illumination intensity at the measured region, but cannot be used for nontransparent substrates. When illuminating the sample from the top, it is important to avoid shadowing of the measured region by the cantilever, which can be either realized by using special probes with tips at the very end of the cantilever, or by illumination at a grazing angle to the sample surface. The drawback of the latter solution is the difficulty of light focusing, which results in a decreased light intensity. Because of the small collecting area underneath the tip, the measured photocurrent is relatively small even for solar cell materials with a very high efficiency. Therefore, high-intensity illumination is

needed, like provided by a laser. The difficulty of using a laser to illuminate the sample is the possible disturbance of the topography measurement, which also employs a laser for detecting the deflection of the cantilever [3,25].

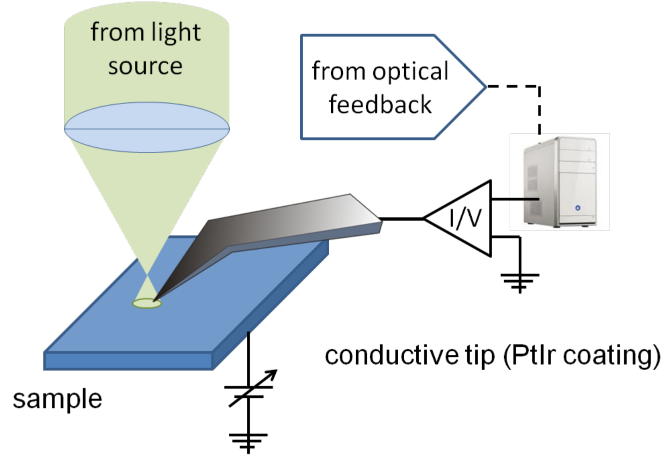

Figure 2.4: Schematic setup of a PC-AFM measurement. To avoid confusion, the feedback laser and diodes of the AFM are not shown. For illumination from the top, special probe geometries have to be used.

2.3.3 Kelvin Probe Force Microscopy

In 1991 Nonnenmacher et al. [4] introduced Kelvin probe force microscopy (KPFM), an AFM method in tapping mode which measures the CPD between the tip and the sample simultaneously with the topography. A scheme of the measurement setup is shown in Fig.2.5. The CPD is the difference in work function between two materials. It depends on many parameters like the adsorbtion layers, oxide layers, dopant concentration and temperature [26,27]. With this method, high lateral resolutions can be achieved for the CPD as well as for the topography, in both cases dependent on the used tip.

The basic principle of KPFM is the Kelvin method, also called vibrating capacitor method [27]. Here, two conducting plates are arranged parallel to each other with a small space in between as a capacitor. The distance between the plates is changed by a periodic vibration with the frequency ω, which results in a current:

$$\mathrm{i(t)} = V_{CPD} \cdot \omega \cdot \Delta C \cdot \cos(\omega t) \tag{2.5}$$

with ΔC the change in capacitance. V_{CPD} can be measured by applying an additional DC voltage between the plates, which reduces the current *i(t)* until it is nullified. The disadvantage of this method is the integration over the whole area of the conducting plates for the CPD-measurement.

In KPFM, an external AC voltage with the frequency ω between the tip and the sample is applied, to create electrostatic forces F_{es}, with the spectral component F_ω at ω [28]:

$$F_{es} = -\frac{1}{2}\frac{\partial C}{\partial z}V^2 \tag{2.6}$$

$$F_\omega = \frac{\partial C}{\partial z}\left(V_{DC} - \frac{\Delta\Phi}{e}\right)V_{AC}\sin(\omega t) \tag{2.7}$$

V_{DC} is the applied DC bias which is needed to annihilate the electric field between the tip and the sample. $\partial C/\partial z$ is the capacitance gradient and $\Delta\Phi/e = (\Phi_{sample} - \Phi_{tip})/e$ is the CPD. The acting force on the cantilever, which is induced by the electric field, is measured to determine the voltage at which the electric field is zero. To neutralize the influence of the topography on the CPD-measurement each line is scanned twice. During the first scan, the topography is imaged in tapping mode. During the second scan, the tip is kept at a constant distance from the previously measured profile and the CPD is measured.

For PA-KPFM, the sample is illuminated during the measurement which causes in semiconductors a photo-induced change in the potential distribution. This surface photovoltage phenomena as well as the photovoltaic effect can be measured with PA-KPFM in tapping mode, which reduces the damage to the sample from the tip. This is very important especially for soft and mechanically instable samples [5].

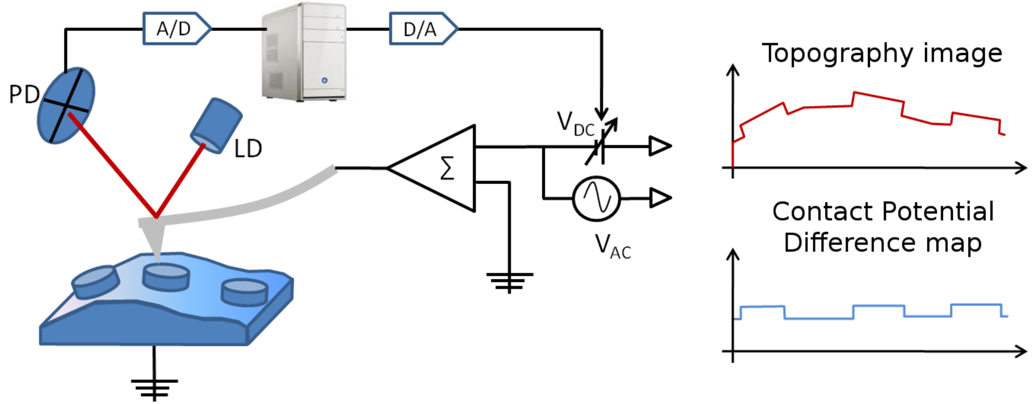

Figure 2.5: Schematic setup of a KPFM measurement. During the first scan of the line the topography image is recorded, during the second scan the tip stays in a constant distance to the previously measured surface, and the CPD is measured.

3 Experimental

3.1 Sample preparation

For all samples, ITO on glass was used as a substrate because of its good electrical conductivity and its transparency.

3.1.1 Spin Coating

For the AnE-PV$_{stat}$: PCBM samples a total mass of 30 mg of the polymers were solved in 1 ml 99.+% chlorobenzene. The solution was spin coated onto the substrate in a glove box. To obtain different film thicknesses, the deposited amount of solution and the rotation speed were varied.

These samples were prepared by Alberto M. Ramil from the group of Prof. Niyazi S. Sariciftci at JKU Linz.

3.1.2 Hot Wall Epitaxy

The C_{60} samples were grown with HWE at the Institute of Physics in Leoben. The corresponding equipment is shown in Fig.3.1. Before the deposition, the substrates were heated in the HWE-chamber in vacuum but outside of the tube at 150℃ for a few minutes to clean the surface without contaminating the tube. After preheating the source at 350℃ and the hot wall at 385℃, the substrate was placed a few centimeters away from the source. For crystalline films the substrate was not cooled and was heated up by the ovens of the source and the hot wall to about 70℃ during the growth. For amorphous films, the substrate temperature was kept at approximately room temperature by cooling with a Peltier element. It was necessary to grow the amorphous film stepwise, since the Peltier element was not efficient enough to keep the substrate temperature low enough during deposition. Therefore, the substrate had to be removed from the tube every 15 minutes. The total deposition time was between 30 minutes and 45 minutes.

For first measurements the samples were prepared by Mujeeb Ullah from the group of Prof. Helmut Sitter at JKU Linz. Later, samples were prepared by Markus Kratzer and the author herself at MU Leoben on substrates provided by Mujeeb Ullah.

3.1.3 Core-Shell Nanoparticles

This nanoparticles were obtained by polymerization of P3MT on the surface of PVDF latex dispersion. These particles can be spun or casted on the substrate to form a film.

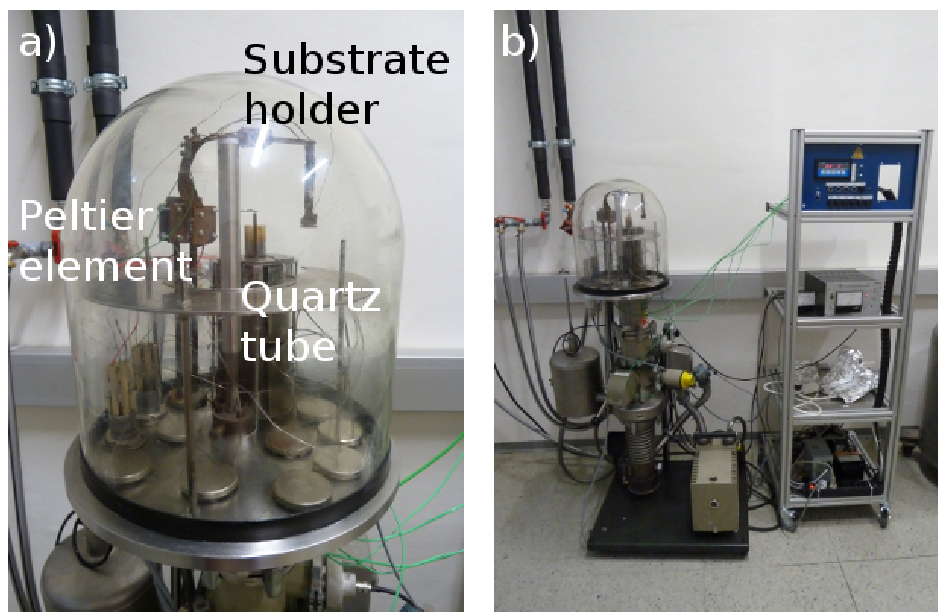

Figure 3.1: The vacuum chamber of the HWE with Peltier element, Quartz tube, and Substrate holder (a). The complete setup including vacuum pumps and electronics (b).

P3HT was used as a binder. For one particular sample, additional PCBM was cast on the film as an attempt to increase the efficiency of the solar cell.

These samples were provided by Valery N. Bliznyuk from the group of Prof. Niyazi S. Sariciftci at JKU Linz.

3.2 Atomic Force Microscopy

All AFM investigations were performed on an Asylum Research (AR) MFP-3D™ system as shown in Fig.3.2 in closed loop configuration. This system has a maximum scan size of 90 μm and a Z-piezo displacement of more than 15 μm. The scanner head is placed on an active damping device to reduce vibrations during the measurement. For KPFM, a standard probe holder from AR was used.

Figure 3.2: Asylum Research MFP-3D™ system at the Institute of Physics in Leoben. Right to the AFM from bottom to top are a Lock-In Amplifier from Stanford Research Systems, an external current preamplifier from DL Instruments and two Keithley 2400 sourcemeters to apply higher sample bias than the MFP can apply.

3.2.1 Current Measurement

The voltage between the organic films and the tip was applied via the MFP-3D™ system. The sign of the applied sample bias characterizes the polarity of the film. For PC-AFM, an external current preamplifier from DL Instruments Model 1211 was employed. With this device, currents of less than a picoampere were measurable with a noise level of about 100 fA. For I-V curve measurements and for some PC-AFM measurements, a modified AR-standard holder with an added current-to-voltage amplifier with a noise level of about 1.5 pA was in use. This device has an offset of -52.5 pA for the current

measurement. All measured current maps are presented with increasing actual current, independent of the sign and the previously mentioned offset. The offset of the modified AR standard probe holder was not subtracted.

3.2.2 Illumination

The samples were illuminated from the top via the optical system of the AFM. For illumination white light was used originating either from a bulb lamp with 150 W or a xenon lamp with 150 W. In both cases, the intensity of illumination was tunable. The emission spectra were measured with a photodiode from Hamamatsu Photonics, and for data evaluation they have been corrected using the calibration curve from the national renewable energy lab (NREL). The corresponding corrected spectra are presented in Fig.3.3. In some cases the sample was illuminated with a light emitting diode (LED) of 490 nm wavelength.

A small influence of the illumination on the topography imaging was observed. This happens because of the influence of the used light on the measurement of the cantilever deflection. In the shown images it has been removed during the flattening process.

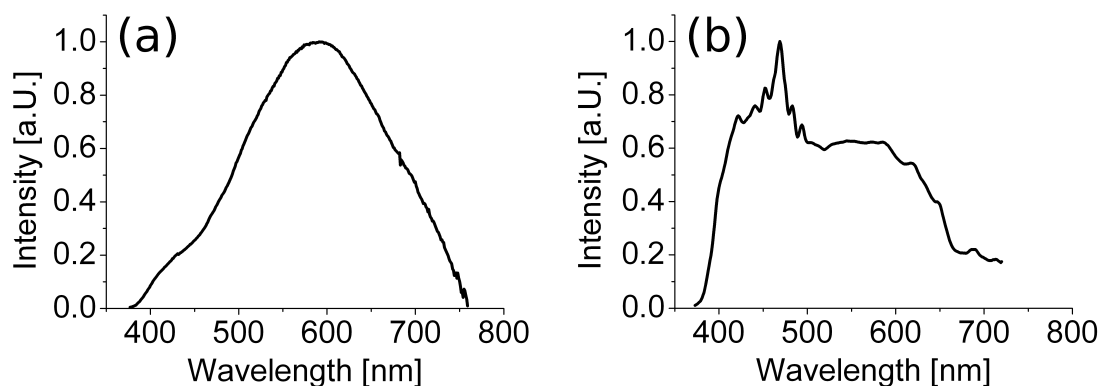

Figure 3.3: Emission spectra of the light sources used for illumination: From the bulb lamp of the optical microscope of the MFP-3D™ (a) and the xenon lamp (b).

3.2.3 Determination of Film Thickness

The thickness of the films was measured by scratching the film with a toothpick. The soft polymer films were easily scored while the ITO is too hard to be damaged by wood. The produced scratch was measured with the AFM and from line scans of the topography image its depth, which resembles the film thickness, was determined.

3.2.4 AFM-Probes

For PC-AFM and PA-KPFM conductive tips and cantilevers are needed. Furthermore, special tip geometries are necessary to ensure an illumination of the measured area when illuminating from the top. These probes have the tip at the very end of the cantilever, pointing slightly to the front. In our case PtIr coated probes from NANOSENSORS™ AdvancedTEC™ (Advanced Tip at the End of the Cantilever) for contact mode (ATEC-Cont) were used for PC-AFM. Probes of the same type for tapping mode (ATEC-NC) were used for PA-KPFM. Fig.3.4 shows a scanning electron microscopy (SEM) micrograph of such a probe. These tips have a tetrahedral shape and a tip radius smaller than 10 nm. The half cone angle at the very end of the tip is smaller than 5°.

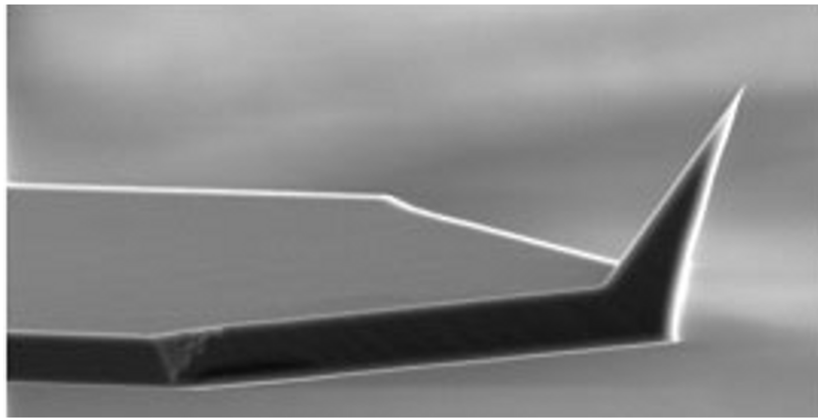

Figure 3.4: SEM image of an AdvancedTEC™ probe from NANOSENSORS™ applicable for PC-AFM and PA-KPFM with illumination from the top. (From [29])

3.2.5 Heating Cell

For some measurements heating of the sample was necessary. Therefore, the PolyHeater™ from AR, presented Fig.3.5, was used. The temperature range of this heating cell is from room temperature up to 250 °C. Most samples had to be measured in inert atmosphere because of a very fast degradation in air. This was realized by filling the closed heating cell with nitrogen. During the measurement the nitrogen flow was kept as low as possible to avoid mechanical oscillations which disturb the AFM measurement. Yet the flow had to be strong enough to maintain a small overpressure in the cell, to ensure that no air can enter the cell through the notches for the wiring.

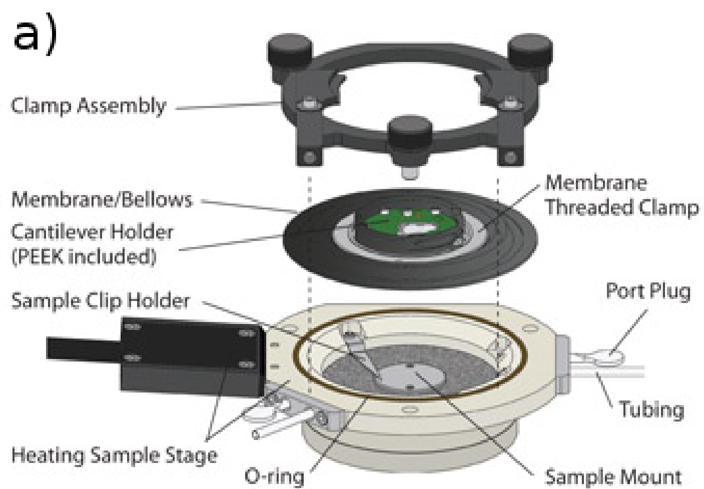

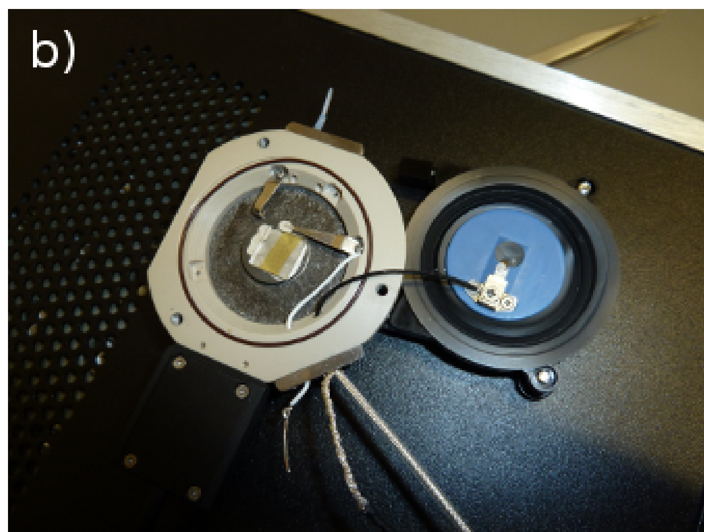

Figure 3.5: A schematic drawing of the polymer heater (from [30]) (a), and an assembled setup with a C_{60} sample and the necessary wiring (b). Additionally, the tube for the nitrogen has to be plugged into the vacant notch.

4 Results

4.1 Organic Solar Cells

4.1.1 AnE-PV$_{stat}$: PCBM

All samples were produced by spin coating in nitrogen atmosphere and transported from Linz to Leoben in nitrogen filled hermetically sealed containers. Samples with different mixture ratios and film thicknesses were analyzed by PC-AFM and PA-KPFM.

Film Thickness $>$ 150 nm

For these samples a bigger amount of solution was put on the substrate and the rotation speed of the spin coating process was smaller. The samples were measured in ambient atmosphere with varying light sources. Different measurement setups were used to obtain more information on the photoelectronic properties of the samples. Due to fast degradation of the samples, it was not possible to analyze each of them by all measurement techniques. Therefore, the adjustments of the measurements for the different samples are not constant.

AnE-PV$_{stat}$: PCBM (1:2) Two samples with the same compounding were measured. The modified AR-standard probe holder and ATEC-Cont probes were used to obtain topography images, current maps and I-V curves. The samples were illuminated by the bulb lamp of the optical system of the AFM.

Fig.4.1.a shows a 5 μm x 5 μm topography image of the first sample, with a film thickness of 210 nm, consisting of particles with a height up to 40 nm and with diameters from 100 nm – 400 nm. The RMS roughness is 5.8 nm for the whole image, for a 2 μm x 2 μm section in the upper right corner the RMS roughness is 5.9 nm. In the corresponding current map Fig.4.1.b recorded at -2 V sample bias a weak photoresponse can be observed, which can also be observed in the corresponding cross-sections (Fig.4.1.c). Under illumination, the average current increases by about 0.3 pA to 48.3 pA and also the noise level increases slightly.

In the topography image, a smoother area can be recognized. Here, the surface was damaged during the previous scan with 2 μm scan size. The square is shifted with respect to the image center due to thermal drift. In this region, the maximum height is about 20 nm and the RMS roughness decreased to 4.5 nm. However, this does not influence the current signal nor the photoresponse.

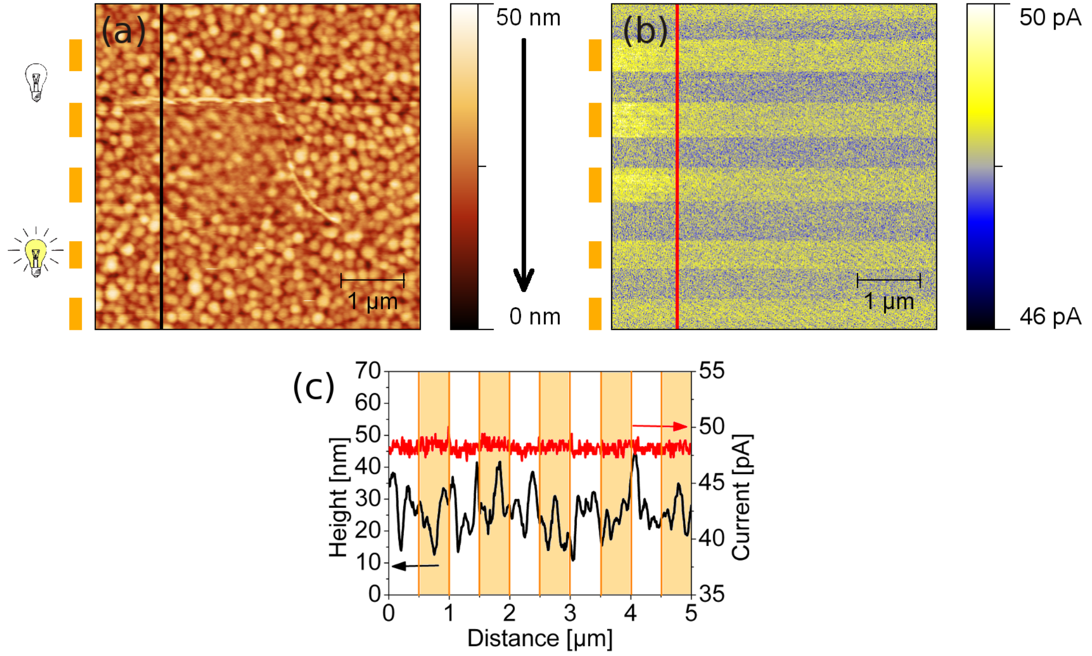

Figure 4.1: 5 μm x 5 μm PC-AFM image of a 210 nm thick AnE-PV$_{stat}$: PCBM (1:2) blend partly illuminated with the bulb lamp, indicated by the orange bars left to the images, measured at room temperature. The scanning direction is from the top to the bottom of the image, indicated by an arrow. Topography (a), current map recorded at -2 V sample bias (b) and the corresponding cross-sections taken along the vertical marked line in scanning direction (c).

The results for the second sample with a film thickness of 200 nm are shown in Fig.4.2. The morphology exhibits particles with a diameter of 100 nm – 300 nm and heights up to 50 nm. The RMS roughness is 8.2 nm. In the current map measured at -2 V sample bias (Fig.4.2.b) and the corresponding cross-sections shown in Fig.4.2.c a clear photoresponse can be observed. This response decreases dramatically during the measurement which can be explained by fast degradation of the sample. At the beginning of the measurement, the dark current had an average value of 48.3 pA and the current under illumination was 53.4 pA. At the end of the scan, after about half an hour, the current under illumination decreased to 48.1 pA while the dark current decreased only slightly by 0.7 pA. The decay of the current signal can be seen in the corresponding cross-sections. The decrease of the current within one scan line from left to right happens due to the sample morphology, and is not influenced by the horizontal scanning direction.

In the current map, also an influence of the topography on the conductivity under illumination can be observed. Some particles with 100 nm – 150 nm in diameter have a lower current signal under illumination, than the rest of the sample, as demonstrated

in Fig.4.2.d. This might be due to irregular distribution of the different polymers in the blend. The dark current is not influenced by the structure of the blend.

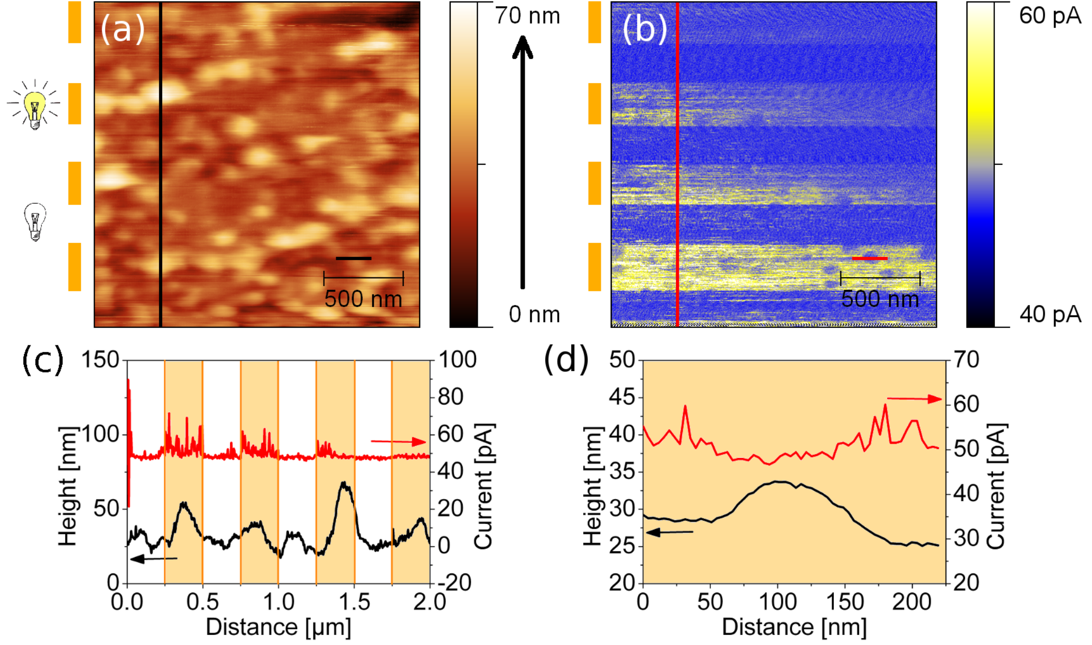

Figure 4.2: 2 μm x 2 μm PC-AFM image of a 200 nm thick AnE-PV$_{stat}$: PCBM (1:2) blend partly illuminated with the bulb lamp measured at room temperature. Topography (a), current map recorded at -2 V sample bias (b), the corresponding cross-sections taken along the vertical marked line in scanning direction (c), and along the short marked line of a less conductive particle under illumination (d). A degradation of the sample during the scanning can be observed in the current map.

Furthermore, on the second sample I-V curves have been measured. At room temperature, neither a dependence on the applied sample bias nor on the illumination can be observed (Fig.4.3.a). At this point of the measurement, the sample is already degraded too much to get any good results. Therefore, the sample was heated up to 100℃ in nitrogen flow and I-V curves have been recorded again, to check, if the sample can be healed by heating. The I-V curves taken at elevated temperature (Fig.4.3.b) show a response on the sample bias and a strong photoresponse can be observed again. At positive bias the increase in current is more pronounced and a hysteresis can be observed. This happens due to the capacitance of the whole setup. The current at 0 V bias is due to the amplifier offset. The current onset for positive bias is already at small voltages slightly above 0 V, and for negative bias the onset is at about -0.4 V. These points are marked on Fig.4.3.b by the blue lines. I-V curves were taken only from -2 V to +2 V sample bias to avoid damaging the film with too high currents.

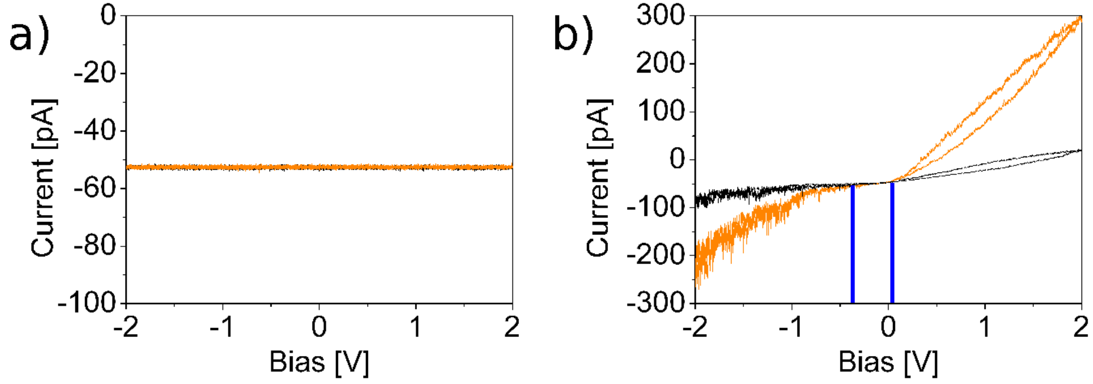

Figure 4.3: I-V curves measured on an arbitrary point on a AnE-PV$_{stat}$: PCBM (1:2) blend under illumination (orange curve) and non illuminated (black curve). At room temperature (a) and at 100°C (b).

AnE-PV$_{\text{stat}}$: PCBM (1:3) For these measurements, the external amplifier from DL Instruments and ATEC-Cont probes were used. The sample was illuminated with varying light sources.

The 2 μm x 2 μm topography image of the measured AnE-PV$_{stat}$: PCBM (1:3) sample with a film thickness of 170 nm, presented in Fig.4.4.a, shows a similar structure as the previous samples with (1:2) ratio. The particles have heights up to 40 nm and diameters of 200 nm – 400 nm. The RMS roughness is 11.2 nm, which is higher than of the previously measured samples, mainly because of the worse quality of the image. In the current map taken at -3 V sample bias shown in Fig.4.4.b, a much higher conductivity of the matrix and almost no conductivity of the particles can be observed. This can also be observed in the short cross-sections over a particle in Fig.4.4.d. The applied sample bias was increased, to analyze, if better results can be achieved with higher voltages. The sample shows no obvious photoresponse (Fig.4.4.c), which might be due to the degradation of the sample during the preceding measurements. This sample was stored in the same nitrogen filled hermetically sealed container, as a previously measured one and therefore was in contact with air some hours before the measurements. Another explanation might be that the material does not react to the 490 nm light which has been used for illumination in this experiment. However, the previous I-V curve measurements at room temperature with illumination by the bulb lamp also show neither a response of the current to light, nor to the applied sample bias within the measured range of ±2 V bias.

AnE-PV$_{\text{stat}}$: PCBM (1:1) This sample was measured with PA-KPFM to investigate the photoelectric properties of the material using a more gentle technique. ATEC-NC probes were used and the sample was illuminated by the bulb lamp of the optical microscope of the AFM from the top.

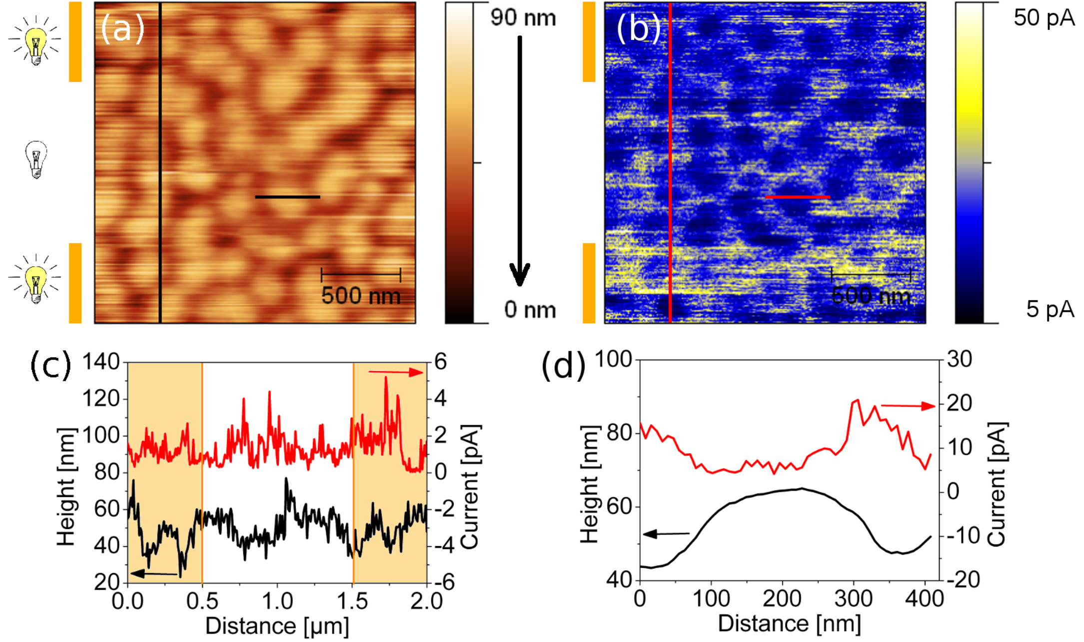

Figure 4.4: 2 μm x 2 μm PC-AFM image of a 170 nm thick AnE-PV$_{stat}$: PCBM (1:3) blend partly illuminated by a LED with 490 nm wavelength measured at room temperature. Topography (a), current map recorded at -3 V sample bias (b), the corresponding cross-sections taken along the vertical marked line in scanning direction (c), and along the short marked line of a less conductive particle without illumination (d).

The average film thickness of this sample is about 260 nm. Fig.4.5 shows an image which was recorded with disabled slow scan axis to investigate the photoresponse independently from the topography. Therefore, the same horizontal scan line was scanned during the whole measurement. The sample was measured at 100℃. A pronounced drop of the CPD in the CPD map can be observed under illumination, which implies an increase of the conductivity of the sample under illumination. After the first cycle of illumination the CPD stayed at a decreased value, compared to the CPD before the sample was illuminated. This phenomena is called persistent photoresponse, where the conductivity stays increased for a while after the illumination of the sample [5]. Furthermore, a higher CPD of the particles can be observed, as demonstrated in Fig.4.5.c & d.

In another measurement, the slow scan axis was only partially disabled, to investigate the CPD of the different components of the sample. The topography image, shown in Fig.4.6.a, reveals much larger structures than on the previously measured one. At the same time the surface fraction of the matrix is higher. The particles are up to 0.2 μm high and have diameters between 200 nm and 2 μm. The RMS roughness of the lower part of the image with enabled slow scan axis is 52 nm. The RMS roughness of an

2 μm x 2 μm section in the lower left corner of the image is 29 nm. In the CPD map (Fig.4.6.b) and the corresponding cross-sections (Fig.4.6.c) a clear photoresponse can be observed again by a reduced CPD. This can also be seen in the corresponding cross-sections. Also the particles have a slightly higher CPD than the matrix, which suggests a lower conductivity. This is consistent with previous PC-AFM measurements. The difference in the CPD, due to the morphology, is less pronounced under illumination, due to a stronger photoresponse of the particles. Differences of the CPD during the measurement without changing the illumination might occur due to a change of the work function of the tip, e.g. by picking up some molecules from the sample, or by damaging the coating of the tip.

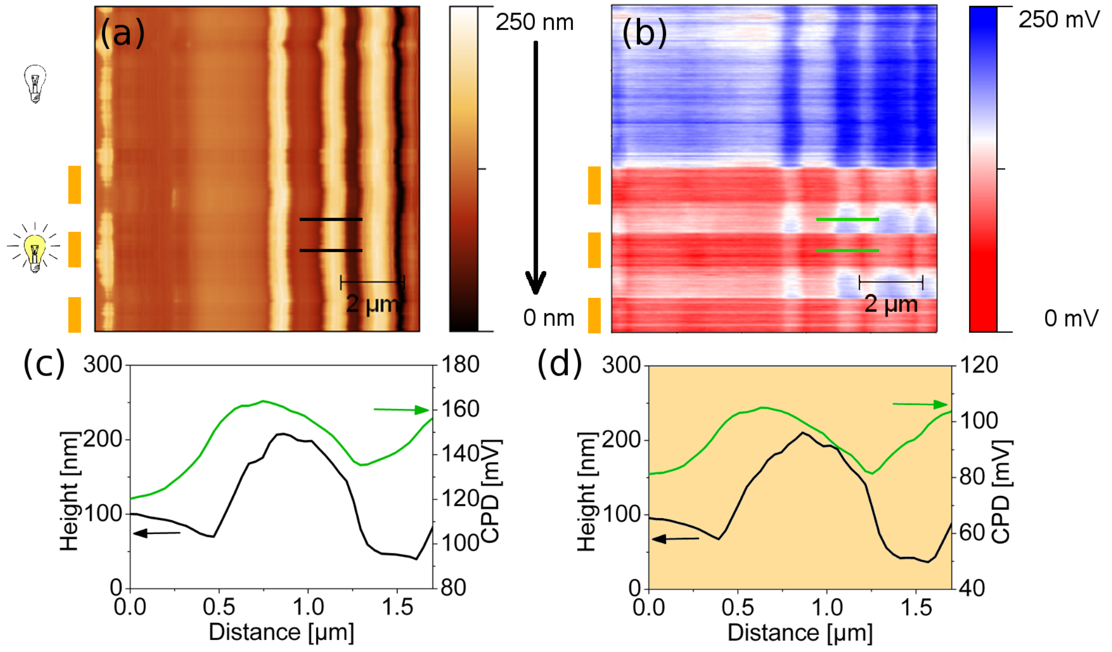

Figure 4.5: 10 μm PA-KPFM measurement of a 260 nm thick AnE-PV$_{stat}$: PCBM (1:1) blend partly illuminated with the bulb lamp measured at 100°C. The scan started at the top. The slow scan axis was disabled, whereby only one scan line was scanned over the whole image. Topography (a), contact potential difference map (b), the corresponding cross-sections taken along the marked lines without illumination (c), and under illumination (d).

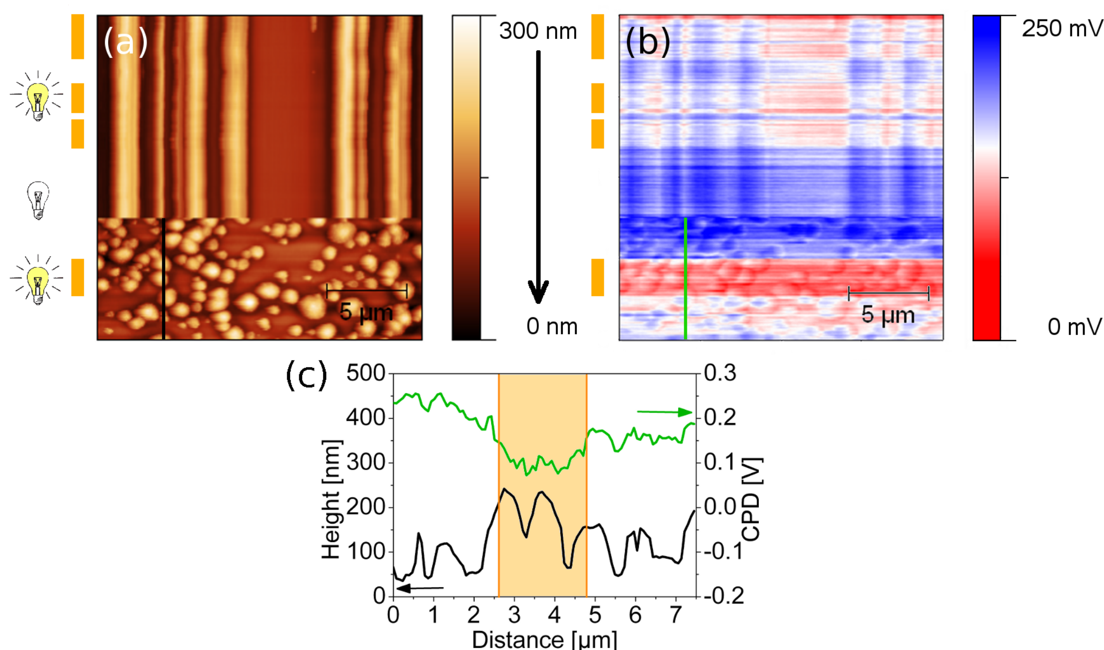

Figure 4.6: 25 μm x 25 μm PA-KPFM image of a 260 nm AnE-PV$_{stat}$: PCBM (1:1) blend illuminated with the bulb lamp measured at 100°C. In the upper part of the image the slow scan axis was disabled. Topography (a), contact potential difference map (b), and the corresponding cross-sections taken along the vertical marked line in scanning direction (c).

Film Thickness < 150 nm

These films were prepared by depositing a smaller amount of solution on the substrate and increasing the rotation speed for the spin coating. After the samples were brought to Leoben, they were stored for some time in nitrogen enriched atmosphere, but no longer in pure nitrogen. They were measured in a nitrogen flow in the opened heating cell and illuminated by the xenon lamp. It was no longer necessary to close the cell, since the samples were already stored in a non inert atmosphere for a longer time.

AnE-PV$_{\text{stat}}$: PCBM (1:3) This sample was measured with the modified AR-standard probe holder and ATEC-Cont probes.

The sample has a film thickness of 90 nm. The topography image measured at room temperature, presented in Fig.4.7.a, shows particles up to 20 nm high and with diameters from 150 nm – 300 nm. These features are slightly smaller compared to the thicker film with the same ratio of components. The RMS roughness is 3.6 nm excluding the contamination in the lower left corner. Neither in the current map measured at +1 V sample bias (Fig.4.7.b), nor in the cross-sections (Fig.4.7.c) a photoresponse can be observed. Here, +1 V sample bias was used, since best results were found under this condition. At the beginning of the scan (in the upper region of the image) the

particles show a lower conductivity than the matrix. This effect vanishes during the scan. The recorded I-V curves, measured on the matrix (Fig.4.7.d), show no response to light, but to the applied sample bias. Apparently, the sample has already degraded during storing in a not completely closed inert atmosphere.

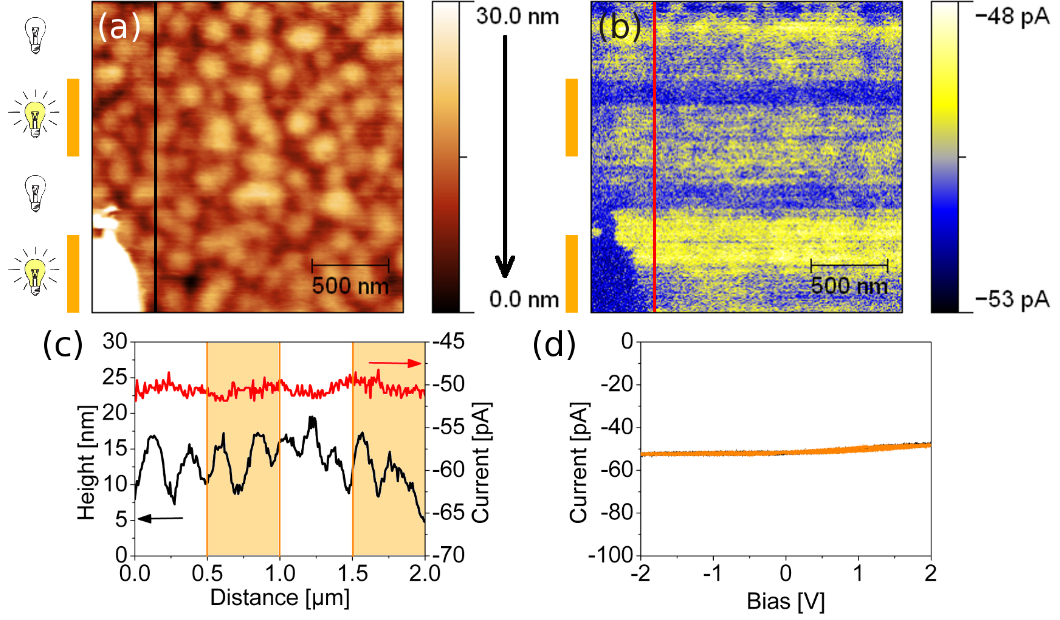

Figure 4.7: 2 μm x 2 μm PC-AFM image of a 90 nm thick AnE-PV$_{stat}$: PCBM (1:3) blend partly illuminated with the xenon lamp measured at room temperature. Topography (a), current map recorded at +1 V sample bias (b), the corresponding cross-sections taken along the vertical marked line in scanning direction (c), I-V curves under illumination (orange), and non illuminated (black) recorded on the matrix (d). In the lower left corner a contamination is visible in the topography and the current map.

To explore if the sample can be healed it was heated up to 100°C and C-AFM as well as I-V curve measurements have been repeated. The results are presented in Fig.4.8. After annealing large mounds of some μm diameter can be found, however the morphology on a smaller scale stayed unchanged. The larger features are analyzed on later samples in more detail. Despite heating of the sample again no response to light can be observed neither in the current map taken at +1 V bias, nor in the I-V curves measured on the matrix, which is shown in Fig.4.8.e, nor on the grains. The I-V curve appears basically ohmic at positive bias voltages. Again the conductivity for negative bias is somewhat lower than for the forward direction. The offset at 0 V is again due to the amplifier characteristic. At higher temperatures the less conductive character of the particles gets more pronounced and the current increases stronger with increasing sample bias. The lower conductivity of the particles can also be observed in the corresponding cross-sections (Fig.4.8.c & d).

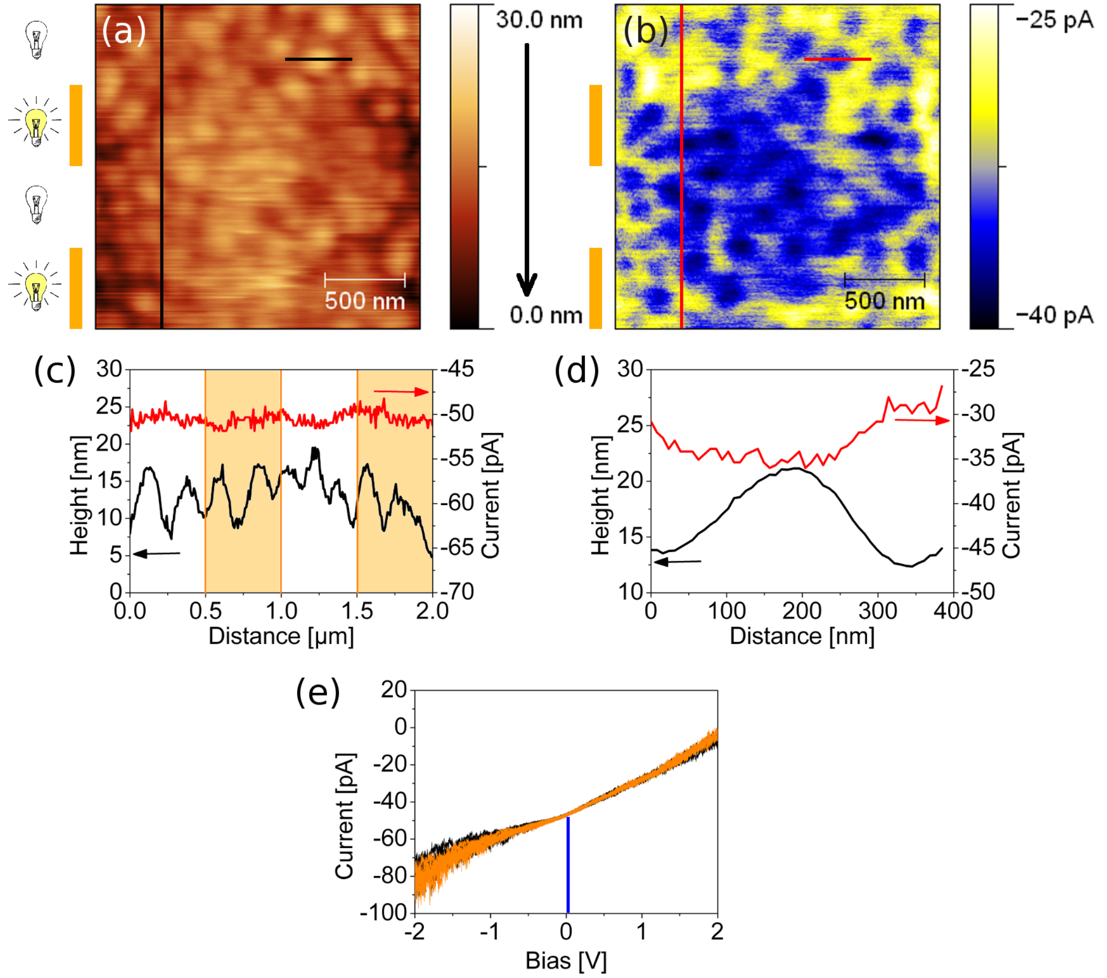

Figure 4.8: 2 μm x 2 μm PC-AFM image of a 90 nm AnE-PV$_{stat}$: PCBM (1:3) blend partly illuminated with the xenon lamp measured at 100°C. Topography (a), current map recorded at +1 V sample bias (b), the corresponding cross-sections taken along the vertical marked line in scanning direction (c), and along the short marked line of a less conductive particle without illumination (d), as well as I-V curves under illumination (orange) and unilluminated (black) recorded on the matrix (e).

AnE-PV$_{\text{stat}}$: PCBM (1:1) For C-AFM and I-V curve measurements the modified AR-standard probe holder and ATEC-Cont probes were used. For PA-KPFM ATEC-NC probes were used.

The sample has a film thickness of 60 nm. Fig.4.9.a shows particles with 40 nm – 100 nm in diameter that are maximum 5 nm high. The morphology is extremely smooth, compared to all the other samples. The RMS roughness of the 1 μm x 1 μm image is about 1 nm. The large structures as seen in the thicker film with (1:1) ratio cannot be observed on this sample with C-AFM. The sample shows neither response

to light in the current map (Fig.4.9.b), nor in the cross-sections (Fig.4.9.c) or the I-V curves measured as well at room temperature as at 100°C (not shown).

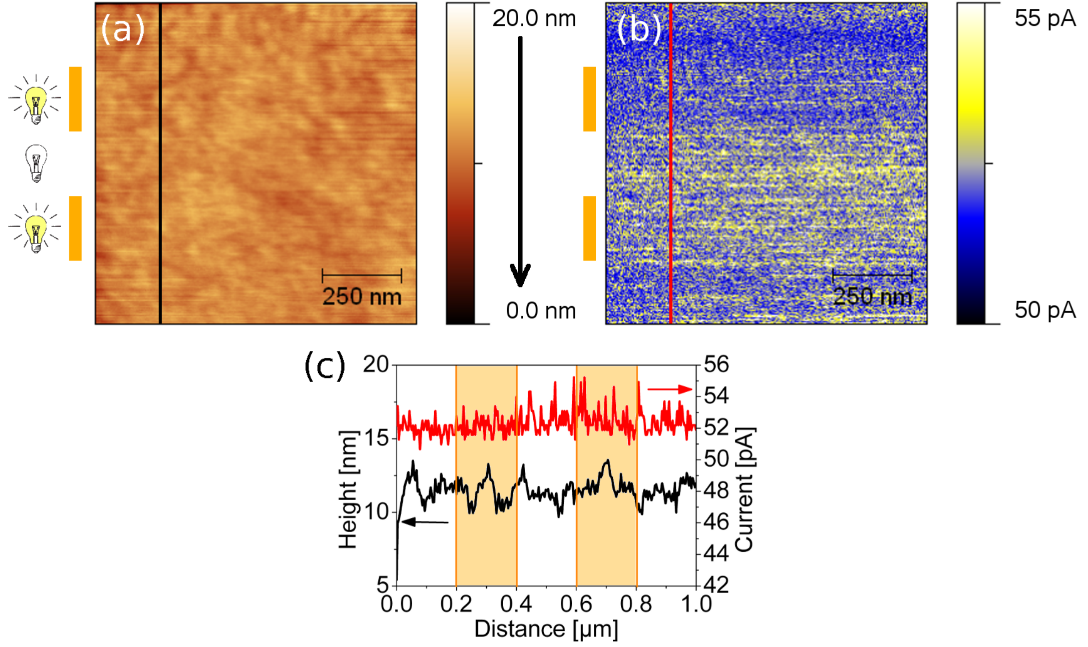

Figure 4.9: 1 μm x 1 μm PC-AFM image of a 60 nm thick AnE-PV$_{stat}$: PCBM (1:1) blend partly illuminated with the xenon lamp and measured at room temperature. Topography (a), current map recorded at -1 V sample bias (b), and the corresponding cross-sections taken along the vertical marked line in scanning direction (c).

After heating up the sample larger features were formed as similar to those observed for the previous samples. Fig.4.10.a shows the KPFM-topography image recorded after heating the sample, where these clusters can be seen more clearly. Their heights are up to 250 nm with diameters of 1 μm – 2 μm. The RMS roughness is 60 nm on the shown image, but the mounds are very inhomogeneously distributed over the sample. In the CPD map no response to light can be observed either at elevated temperature nor at room temperature (Fig.4.10.b). In both cases the matrix has a lower CPD than the particles, which is in agreement with the thicker film. This can also be observed in the corresponding cross-sections (Fig.4.10.c & d). The average CPD of the matrix is 250 mV and of the particles about 350 mV.

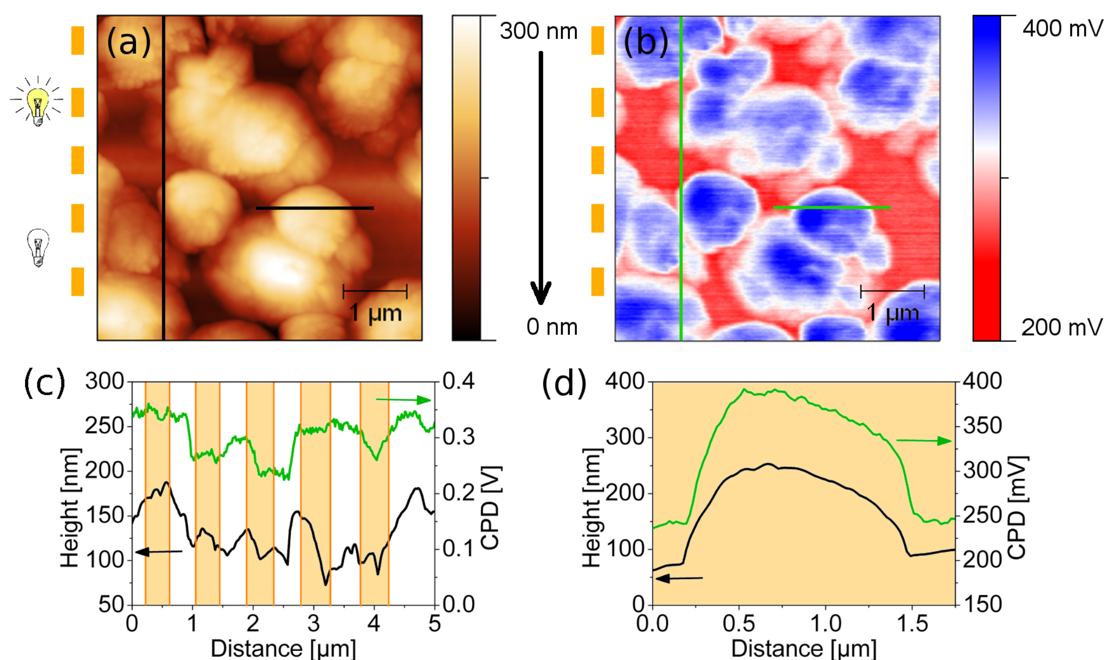

Figure 4.10: 5 μm x 5 μm PA-KPFM image of a 60 nm AnE-PV$_{stat}$: PCBM (1:1) blend partly illuminated with the xenon lamp, measured at room temperature after annealing to 100℃. Topography (a), contact potential difference map(b), the corresponding cross-sections taken along the vertical marked line in scanning direction (c), and along the short marked line of a less conductive particle under illumination (d).

4.1.2 PVDF-P3MT/P3HT : PCBM

These samples were measured in air at room temperature with PC-AFM. All samples were illuminated with the bulb lamp of the optical system of the MFP-3D AFM. For the current measurements, the external preamplifier from DL Instruments and ATEC-Cont probes were used. All measured films are deposited on a Poly(3,4-ethylenedioxythiophene) (PEDOT) layer on the ITO substrate.

PVDF-P3MT core-shell nanoparticles with P3HT binder on PEDOT The topography images of this sample are blurry because the sample surface was mechanically not stable enough for the AFM measurements in contact mode.

The sample has a film thickness of 260 nm. Fig.4.11.a shows particles with 150 nm – 350 nm in diameter and up to 6 nm high. The RMS roughness is 1.4 nm. The current map taken at +2 V sample bias (Fig.4.11.b) shows a current increase due to illumination. This can also be observed in the corresponding cross-sections (Fig.4.11.c). The average value of the dark current is 0.17 nA, while the average current under illumination is 0.22 nA. The noise increases under illumination slightly as well. On the matrix a lower current was measured compared to the particles.

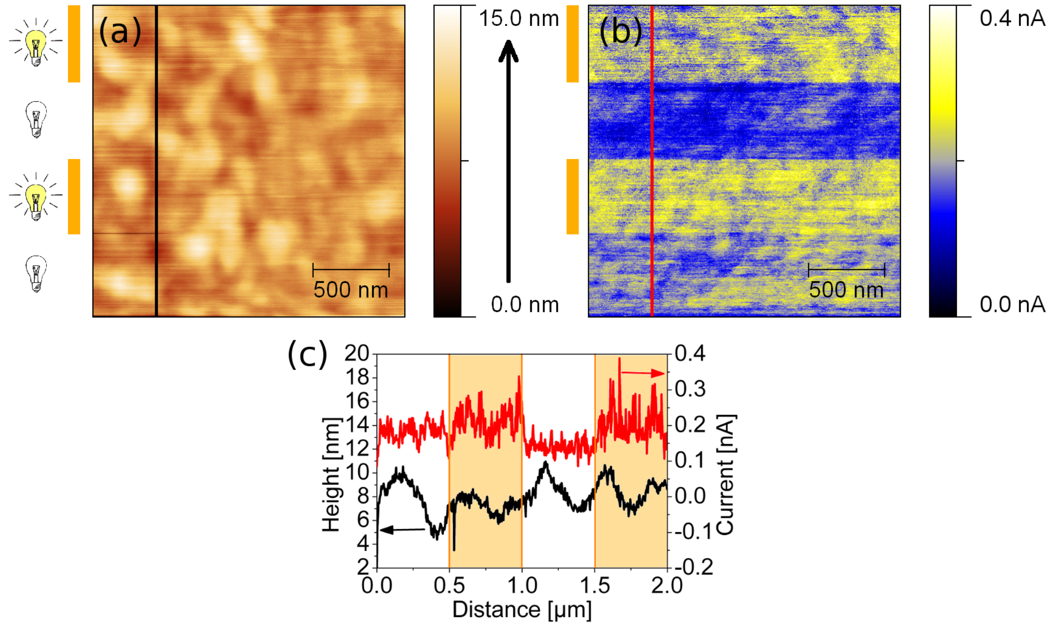

Figure 4.11: 2 μm x 2 μm PC-AFM image of PVFD-P3MT core-shell nanoparticles with P3HT binder partly illuminated with the bulb lamp measured at room temperature. The film thickness is 260 nm. Topography (a), current map recorded at +2 V sample bias (b), and the corresponding cross-sections taken along the vertical marked line in scanning direction (c).

In Fig.4.12, taken at the same position as the previous image, the particles seen in the topography image are slightly larger. The diameters reach from 200 nm – 400 nm and the height is up to 10 nm. The RMS roughness is 1.9 nm and is increased compared to the previous scan. Either the distribution of particles on the sample is not homogeneous, or the features seem to be larger due to the fuzzier image. In the current map taken at -2 V bias (Fig.4.12.b) a persistent photoresponse [5] can be observed. The current does not drop to the dark current value right after turning off the light, but decreases slowly with time. The bias was changed to observe the influence of the applied sample bias on the measurement. The currents measured are in the same range, as with positive sample bias. The average dark current before illumination is about 90 pA, under illumination the value increases to 250 pA. At the end of the measurement, about half an hour after switching off the light, the current decreases to 175 pA (Fig.4.12.c).

Fig.4.13 was measured on a sample with a film thickness of 170 nm. The topography shows smaller features with particles up to 5 nm in height and 100 nm – 250 nm in diameter. The RMS roughness is with 1.7 nm similar to that of the thicker film. In the current image only a week response to light can be observed at $\pm$10 V applied sample bias. This can also be observed in the corresponding cross-sections in Fig.4.13.c. Due to the bad quality of the image no influence of the morphology on the current can be determined.

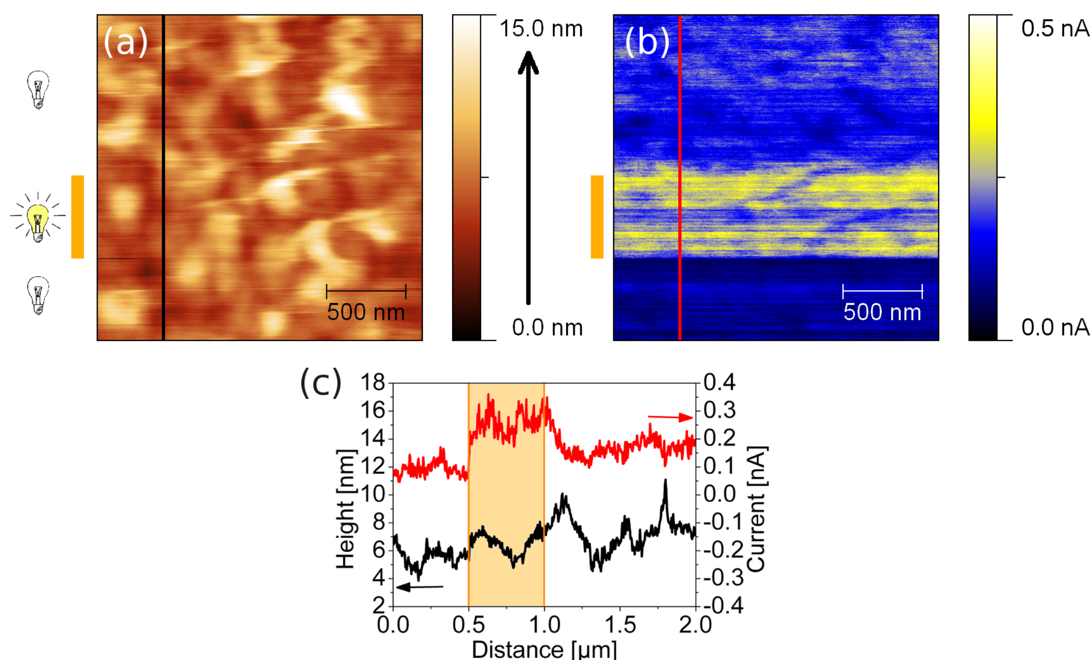

Figure 4.12: 2 μm x 2 μm PC-AFM image of PVFD-P3MT core-shell nanoparticles with P3HT binder on PEDOT partly illuminated with the bulb lamp and measured at room temperature. The film thickness is 260 nm. Topography (a), current map recorded at -2 V sample bias (b), and the corresponding cross-sections taken along the vertical marked line in scanning direction (c).

PVDF-P3MT core-shell nanoparticles with P3HT binder and PCBM drop cast on PEDOT This sample with a film thickness of 200 nm, presented in Fig.4.14, seems to be a bit smoother with particles of up to 300 nm in diameter and 4 nm height. The RMS roughness is 0.8 nm. The sample shows a response to light and the dark current, as well as the current under illumination are by at least one magnitude higher, than of the sample without PCBM drop cast and the higher film thickness. The average dark current is 5.2 nA and the average current under illumination 6.3 nA. The particles seem to have a lower conductivity, but the topography image is too blurry to get good results, but in the corresponding cross-sections, presented in Fig.4.14.c & d, an influence of the morphology on the current signal can be observed.

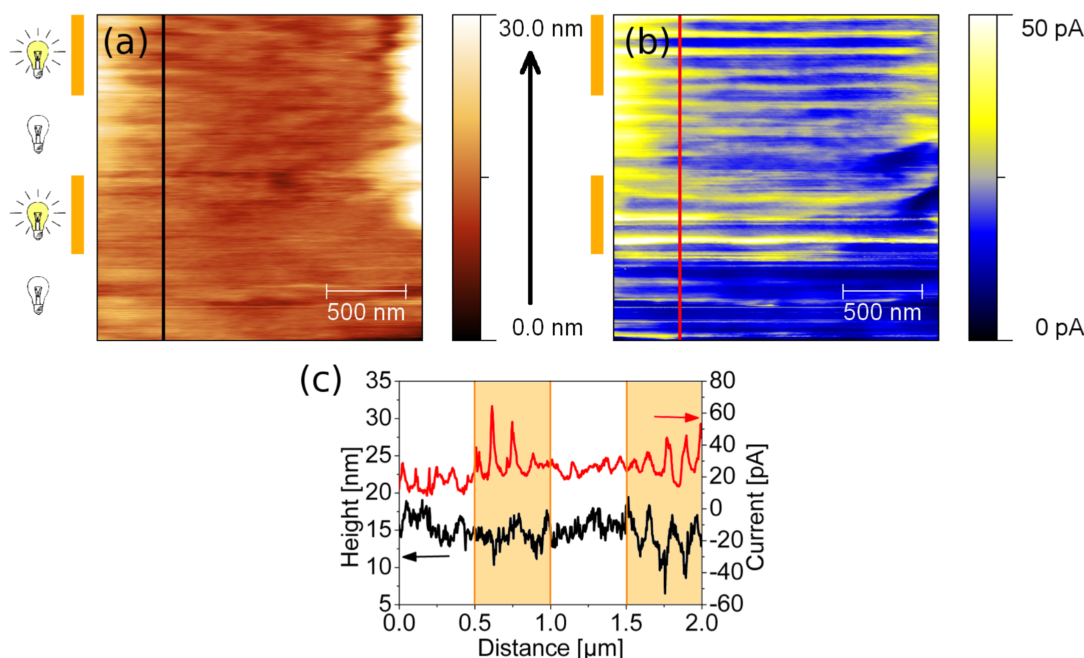

Figure 4.13: 2 μm x 2 μm PC-AFM image of PVFD-P3MT core-shell nanoparticles with P3HT binder on PEDOT partly illuminated with the bulb lamp and measured at room temperature. The film thickness is 170 nm. Topography (a), current map recorded at +10 V sample bias (b), and the corresponding cross-sections taken along the vertical marked line in scanning direction (c).

P3HT : PCBM (1:1) on PVDF The PVDF-film was deposited from the solution and the P3HT: PCBM blend was spin coated.

The first sample has a film thickness of 250 nm. The topography image, presented in Fig.4.15.a, is very blurred, because of the instability of the film even with very low tip loads for the AFM measurements in contact mode. The current map (Fig.4.15.b), as well as the corresponding cross-sections (Fig.4.15.c) show a clear increase of the current on illumination. The average value of the dark current is 90 pA, whereas photocurrent equals 110 pA. For the evaluation of the dark current the less conductive region at the bottom of the image was not taken into account. This jump in the current map happened without any changes of the measurement parameters, and during rescanning, this was observed again. Therefore, the change in conductivity might be attributed due to a inhomogeneity in the sample. The average value of the current measured in this region is about 15 pA.

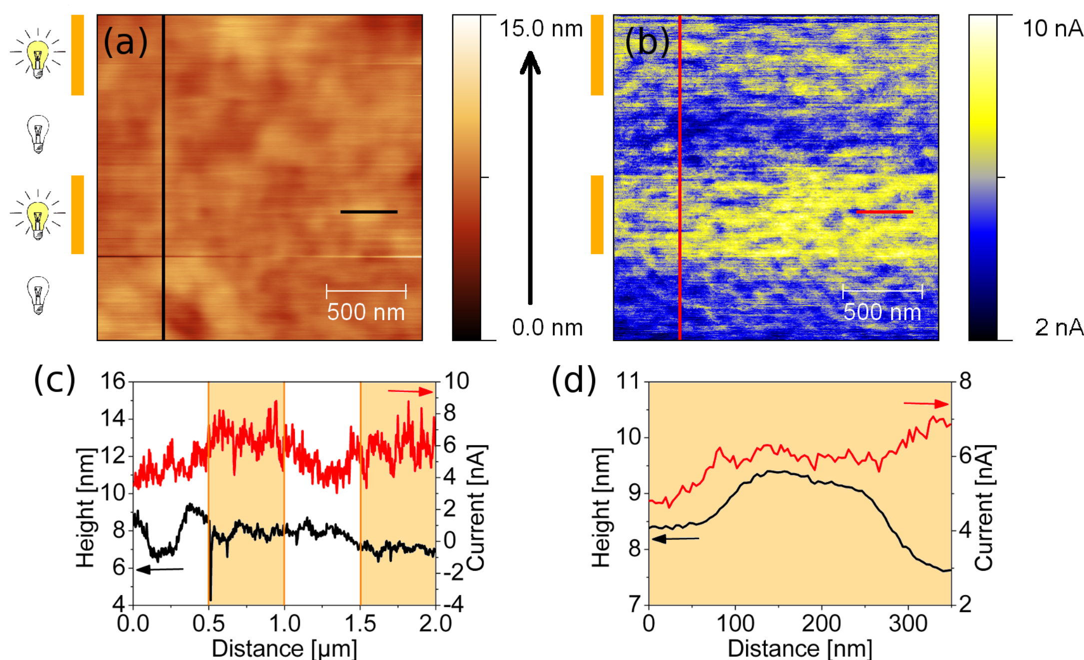

Figure 4.14: 2 μm x 2 μm PC-AFM image of PVFD-P3MT core-shell nanoparticles with P3HT binder and PCBM drop cast on PEDOT partly illuminated with the bulb lamp and measured at room temperature. The film thickness is 200 nm. Topography (a), current map recorded at -2 V sample bias (b) and the corresponding cross-sections taken along the vertical marked line in scanning direction (c), and along the short marked line of a less conductive particle under illumination (d).

For the second sample with a film thickness of 100 nm, the topography can not be measured with AFM in contact mode any more. Neither a current without illumination nor under illumination can be measured. Even at $\pm$10 V sample bias the current image shows only noise. From time to time after changing the bias some current can be measured, but not for a whole scan. However, under illumination the noise ratio of the current signal increases compared to the measurement without illumination. With the optical microscope of the MFP-3D™ different colored regions on the film can be seen, which might indicate varying thicknesses of the film. Measurements on the different regions show no changes in the current signal, neither does the topography imaging improve.

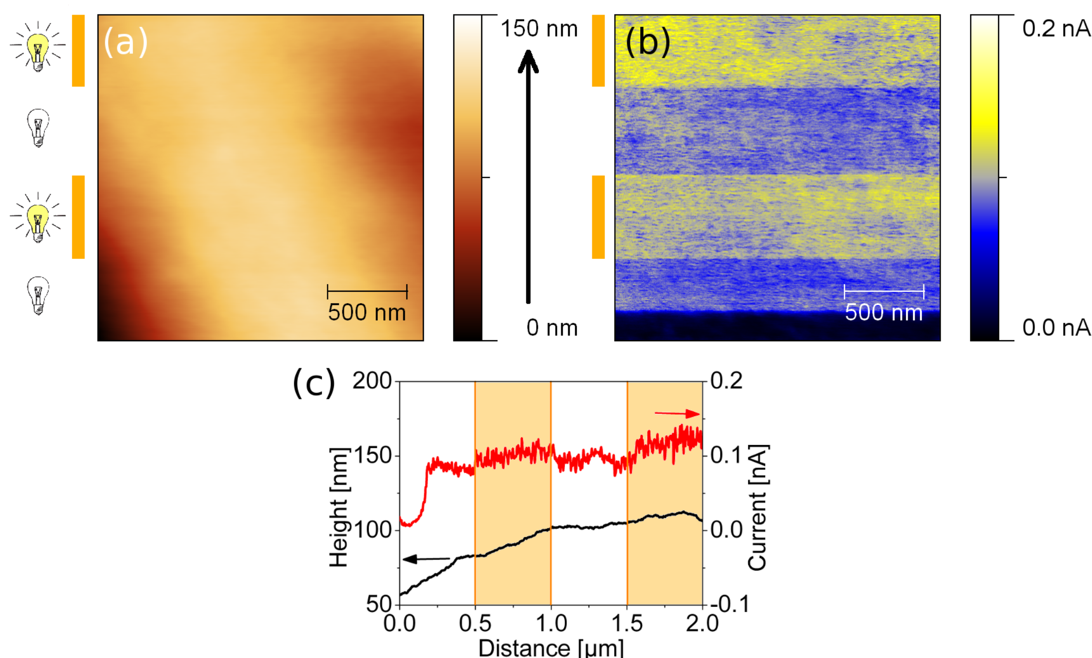

Figure 4.15: 2 μm x 2 μm PC-AFM image of an P3HT : PCBM (1:1) blend on PVDF partly illuminated with the bulb lamp and measured at room temperature. The film thickness is 250 nm. Topography (a), current map recorded at +2 V sample bias (b), and the corresponding cross-sections taken along the marked line in scanning direction (c).

PVDF-P3MT core shell nanoparticles on PEDOT The PC-AFM measurements of this sample with a film thickness of 1.3 μm damaged the surface too much, to get any good images. The measurements were only stable for a few scan lines and after that the particles on the sample were shifted by the tip. Therefore, no usable image could be taken to analyze the topography of the sample and on the current maps no photoresponse was observed. For further investigations PA-KPFM was applied utilizing ATEC-NC probes. In Fig.4.16 the topography shows rather big clusters of particles. The clusters are up to 0.6 μm high and 4 μm long. The particles have diameters of 100 nm – 600 nm and heights of up to 100 nm. The RMS roughness obtained from the 5μm x 5μm image is about 180 nm. Neither the CPD map (Fig.4.16.b), nor the cross-sections (Fig.4.16.c) show a photoresponse of the sample, similar to the current maps recorded with PC-AFM. However, a lower CPD of the matrix compared to the particles can be observed, which suggests a higher conductivity of the matrix.

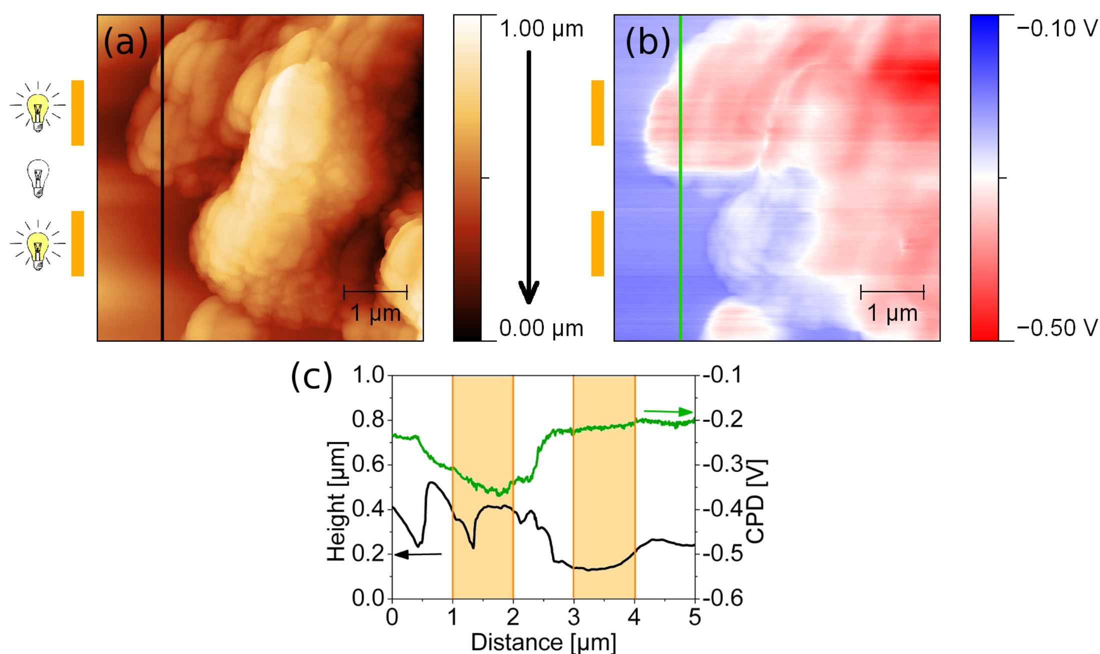

Figure 4.16: 5 μm x 5 μm PA-KPFM image of PVDF-P3MT core-shell nanoparticles partly illuminated with the bulb lamp and measured at room temperature. The film thickness is 1.3 μm. Topography (a), contact potential difference map (b), and the corresponding cross-sections taken along the vertical marked line in scanning direction (c).

PVDF-P3MT core-shell nanoparticles : PCBM (2:1) on PEDOT Similar to the PVDF-P3MT core-shell nanoparticles on PEDOT, this sample with a film thickness of 2 μm is mechanically to instable to obtain any good images with PC-AFM. Also the current maps show no response to light at all. With PA-KPFM the topography of the sample can be analyzed much better, unfortunately, the tip used for this measurements already had a double tip. Therefore, the features are measured twice in the topography image. However, on the CPD map, presented in Fig.4.17.b, no response to light can be observed either. The same result one gets from the cross-section taken along the slow scan axis (Fig.4.17.c). The topography image shows again clusters with up to 5 μm in diameter and 0.8 μm height, consisting of particles with diameters between 200 nm – 700 nm and 150 nm height. The RMS roughness of the image shown is about 200 nm.

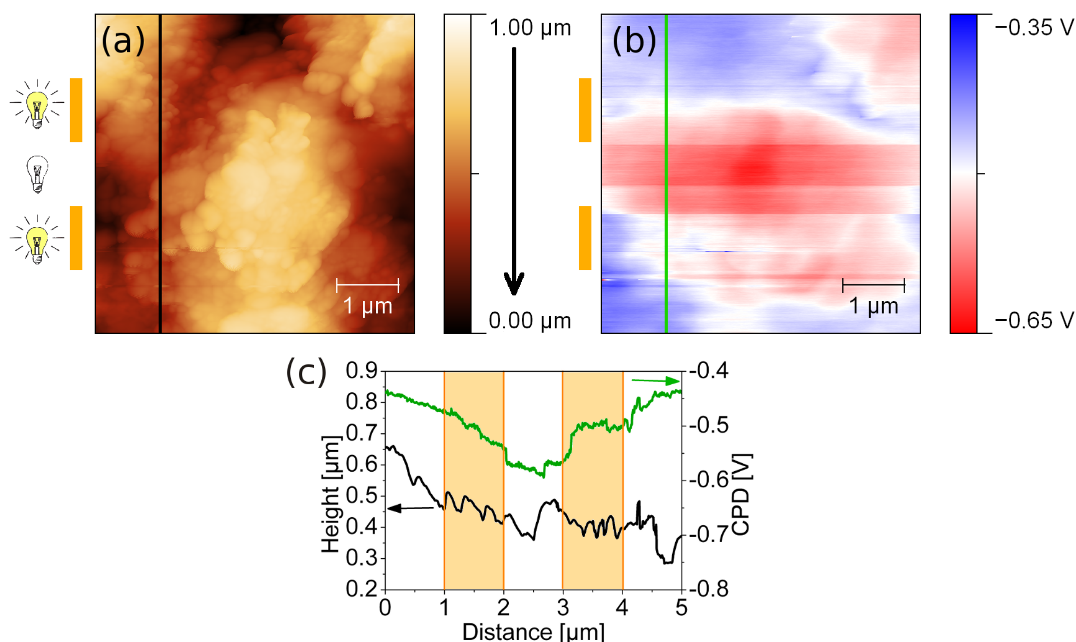

Figure 4.17: 5 μm x 5 μm PA-KPFM image of a PVDF-P3MT core-shell nanoparticles : PCBM (2:1) blend partly illuminated with the bulb lamp and measured at room temperature. The film thickness is 2 μm. Topography (a), contact potential difference map (b), and the corresponding cross-sections taken along the vertical marked line in scanning direction (c).

P3HT with PVDF nanoparticles on PEDOT This sample consists of PVDF particles, which are supposed to have a diameter of about 200 nm, embedded in a P3HT matrix. The average film thickness is 300 nm.

Since no stable conditions for the PC-AFM measurements could be obtained, the sample was also analyzed with PA-KPFM and ATEC-NC probes were used. In the PC-AFM measurements no clear topography image could be recorded. Therefore, the current signals of the different components of the blend can not be compared. Additionally, no response to light can be observed in the current maps.

The topography image of the PA-KPFM measurement, presented in Fig.4.18.a, shows particles with diameters of about 100 nm – 200 nm and heights of up to 30 nm. These particles form bigger clusters with about 1 μm in diameter and 0.1 μm height. The RMS roughness of the presented image is about 60 nm. The coverage of the particles on the matrix changes significantly over the sample. At some points single particles, all with a diameter of about 200 nm can be observed. These sizes are comparable with the sizes, the PVDF particles are supposed to have. The CPD map (Fig.4.18.b) and the vertical cross section (Fig.4.18.c) show no response to light on the conductivity. However, smaller clusters with diameters of less than 1 μm seem to have a lower CPD than others. This can also be seen in the corresponding cross-sections of the topography and the CPD-map in Fig.4.18.d.

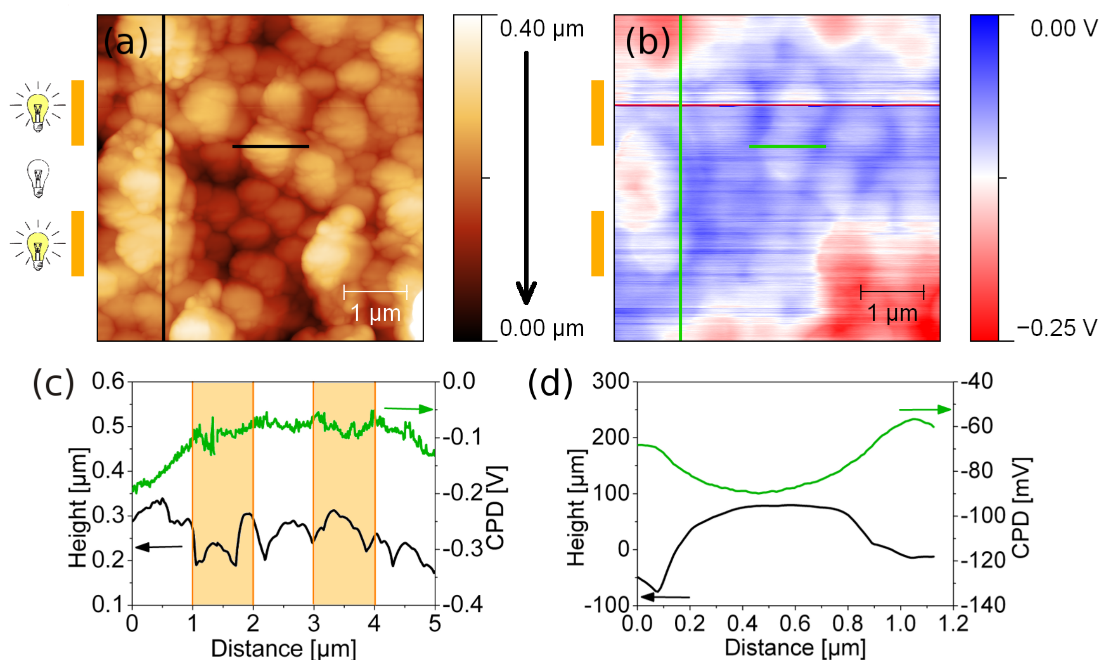

Figure 4.18: 5 μm x 5 μm PA-KPFM image of P3HT with PVDF nanoparticles partly illuminated with the bulb lamp and measured at room temperature. The average film thickness is 300 nm. Topography (a), contact potential difference map (b), the corresponding cross-sections taken along the vertical marked line in scanning direction (c), and along the short marked line of a cluster with lower CPD without illumination (d).

4.2 The Meyer-Neldel Rule on C_{60} films

Different C_{60} films were grown with HWE under varying growth conditions. These films were analyzed using the external amplifier from DL Instruments and ATEC-Cont probes. The samples were illuminated from the top with the xenon lamp and the intensity was either adjusted by filters or by changing the width of a slit placed between the lamp and the glass fiber. The samples were measured in the closed heating cell filled with nitrogen. The setup is illustrated in Fig.4.19. The first measurements were done on samples prepared by Mujeeb Ullah in Linz and transported to Leoben under ambient conditions. For obtaining decent results these samples were already too much degraded. To reduce degradation in air before the measurements, subsequent samples were prepared in Leoben and transferred from the vacuum chamber to the nitrogen filled heating cell immediately. Additionally, the properties of the film at two different temperatures were measured within one scan, to avoid too much changes of the properties during the measurements due to degradation. Therefore, strong thermal drifting can be observed in the middle of all images.

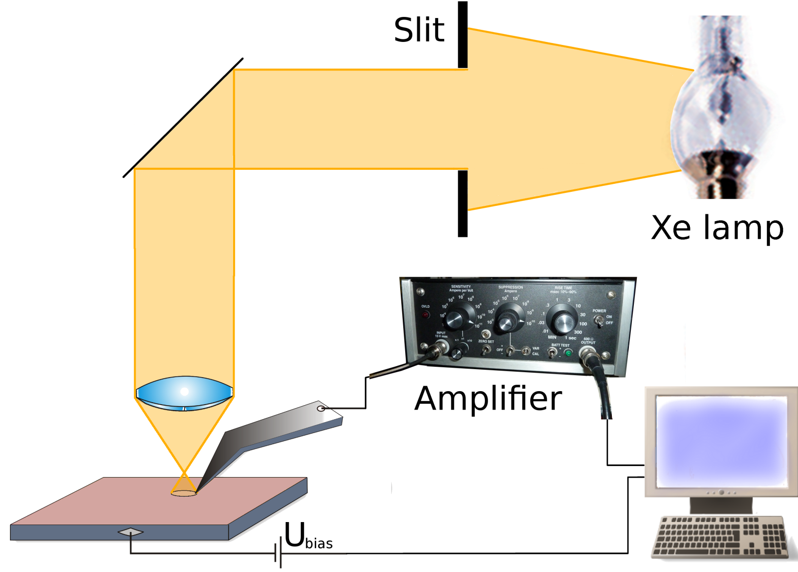

Figure 4.19: Setup of the measurements on C_{60} thin films with ATEC-Cont probes, the external preamplifier, the xenon lamp, and an adjustable slit.

For the investigation of the MNR on the C_{60} films the average current values of the differently illuminated regions are analyzed. For the calculation of the current density, an effective contact area A_{eff} of 24 nm^2 was estimated by [31]:

$$A_{eff} = \pi r_c^2 \tag{4.1}$$

$$r_c^3 = \frac{3}{4}\left(k_1 + k_2\right) F_{ts} R_{tip} \tag{4.2}$$

$$k_i = \frac{1 - \nu_i}{E_i} \tag{4.3}$$

with A_{eff} the effective contact area between tip and sample, r_c the contact radius, F_{ts} the force between tip and sample, R_{tip} the tip radius, and k_i material parameters, which depend on the Young's modulus E_i [32] and the Poisson's ratio ν_i [32] of the material.

The activation energy (E_A) was determined by measuring the slope of the curves in the Arrhenius Plots and calculating it by:

$$E_A = -\frac{\Delta lnj}{\Delta 1/T}\frac{k_B}{e} \tag{4.4}$$

with E_A in eV, $\frac{\Delta lnj}{\Delta 1/T}$ the slope of the curve, k_B the Boltzmann constant and e the elementary charge.

Crystalline Film

The crystalline film was grown with a source temperature of 350°C and a wall temperature of 385°C. The substrate was not cooled and the temperature increased up to 70°C during the growth. The deposition time was 30 minutes. C_{60} films grown under these conditions are usually polycrystalline with a face centered cubic (fcc) structure with poor cristallinity [33,34].

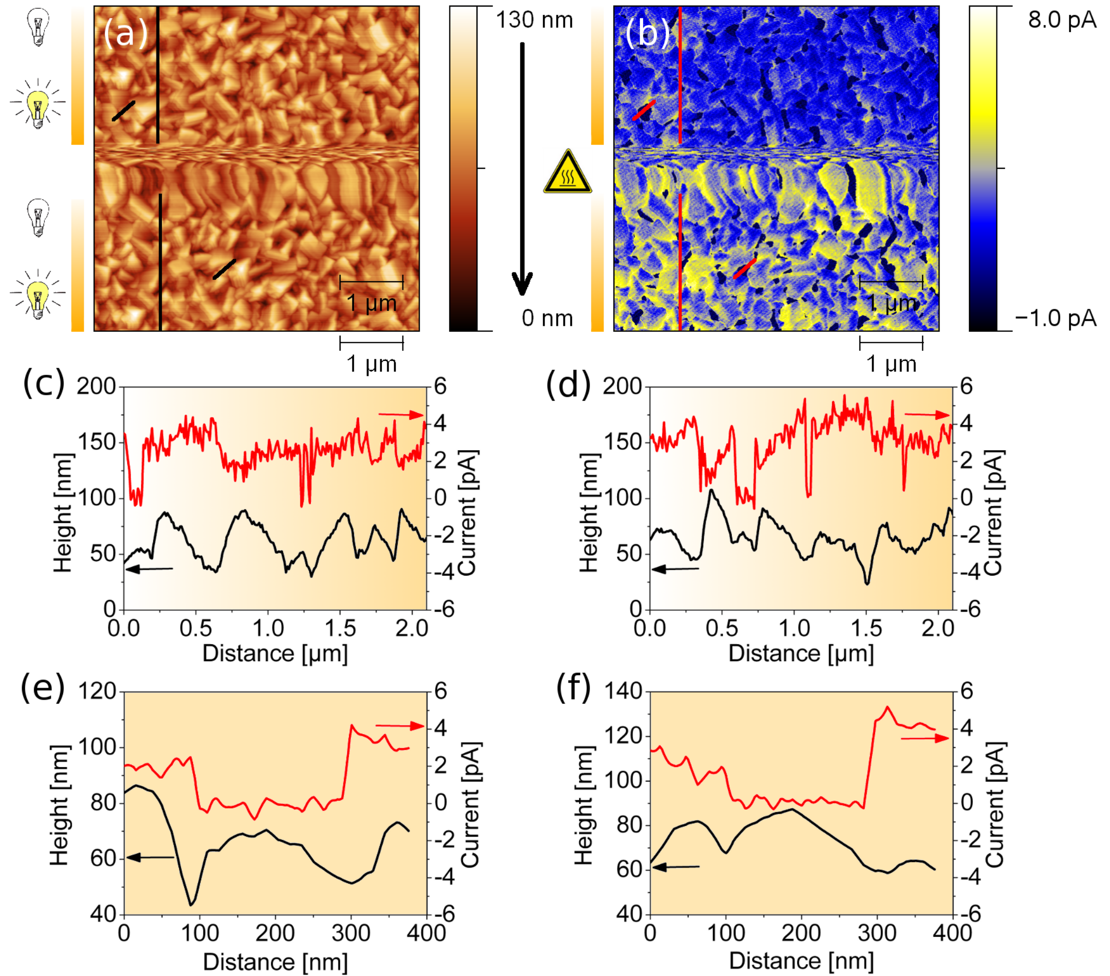

Figure 4.20: 5 μm x 5 μm PC-AFM image of a 800 nm thick crystalline C_{60} film under increasing intensity of illumination of the xenon lamp. In the upper part, the sample is at 100°C, in the lower part at 110°C. Topography (a), current map recorded at -2 V sample bias (b), the corresponding cross-sections taken along the vertical marked lines at 100°C (c) and 110°C (d), and the cross-sections of single non-conductive grains taken along the short marked lines at 100°C (e) and at 110°C (f).

The topography image, presented in Fig.4.20.a, shows crystallites up to 80 nm in height and 700 nm long. Multiple layers can be observed on the steeper edges of the crystallites. The angles between the facets are about 120° – 140°, which might be increased due to the influence of the tip geometry with an opening angle of less than 10° on the topography measurement. The surface has an RMS roughness of 16 nm. The thickness of the film is about 800 nm, which is in the same size range, as the length of the crystallites. The temperature was 100℃, in the middle of the image it was increased to 110℃.

In the current image (Fig.4.20.b), a strong reaction of the current to the sample temperature can be observed. However, neither on the current map, nor on the cross-sections taken along the slow scan axis (Fig.4.20.c & d) an influence to the change of the illumination intensity can be noticed. On some individual grains, almost no current can be measured. The topography and current cross sections of such grains are shown at different temperatures (Fig.4.20.e at 100℃ and Fig.4.20.f at 110℃). Due to the high crystallinity of the film and the rather big crystallites, not all grains seem to be in good electrical contact with each other. This results in the observed non conductive grains.

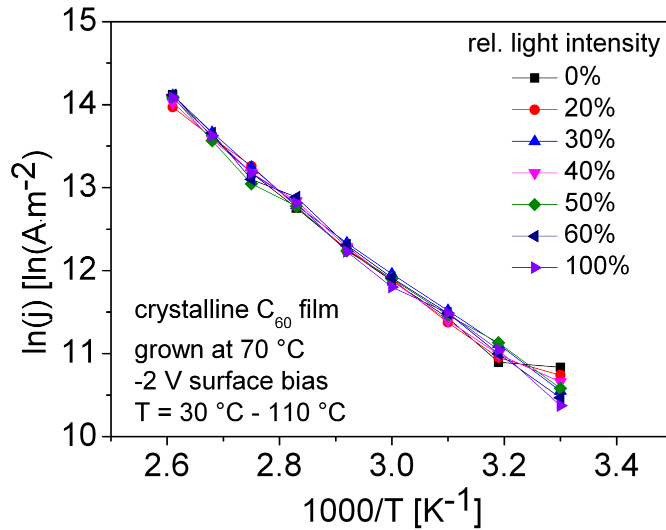

Figure 4.21: Analysis of the evaluated data of a crystalline 800 nm thick C_{60} film. Arrhenius plots of the current density over the inverse temperature under different degrees of illumination.

Fig.4.21 shows the Arrhenius plots of the current densities over the inverse temperature at seven different degrees of illumination. The mean current was determined by averaging the current in the section with the corresponding light intensity. The curves are almost linear, which matches to the theory and to previously macroscopically measured data [20]. The response to light is too little, to be observable, therefore the T_{MN} cannot be determined. Also previous studies have shown that with increasing

crystallinity of the C_{60} film the T_{MN} shifts to lower temperatures [20]. Thus, in our case this point might be below the temperature range we were able to investigate. The slope of the curve is about -5000 K and the calculated E_A is 0.43 eV.

Partly Crystalline Film

This film was grown for 45 minutes with a source temperature of 350℃ and a wall temperature of 385℃. The substrate was cooled with the Peltier element and the temperature was about 50℃.

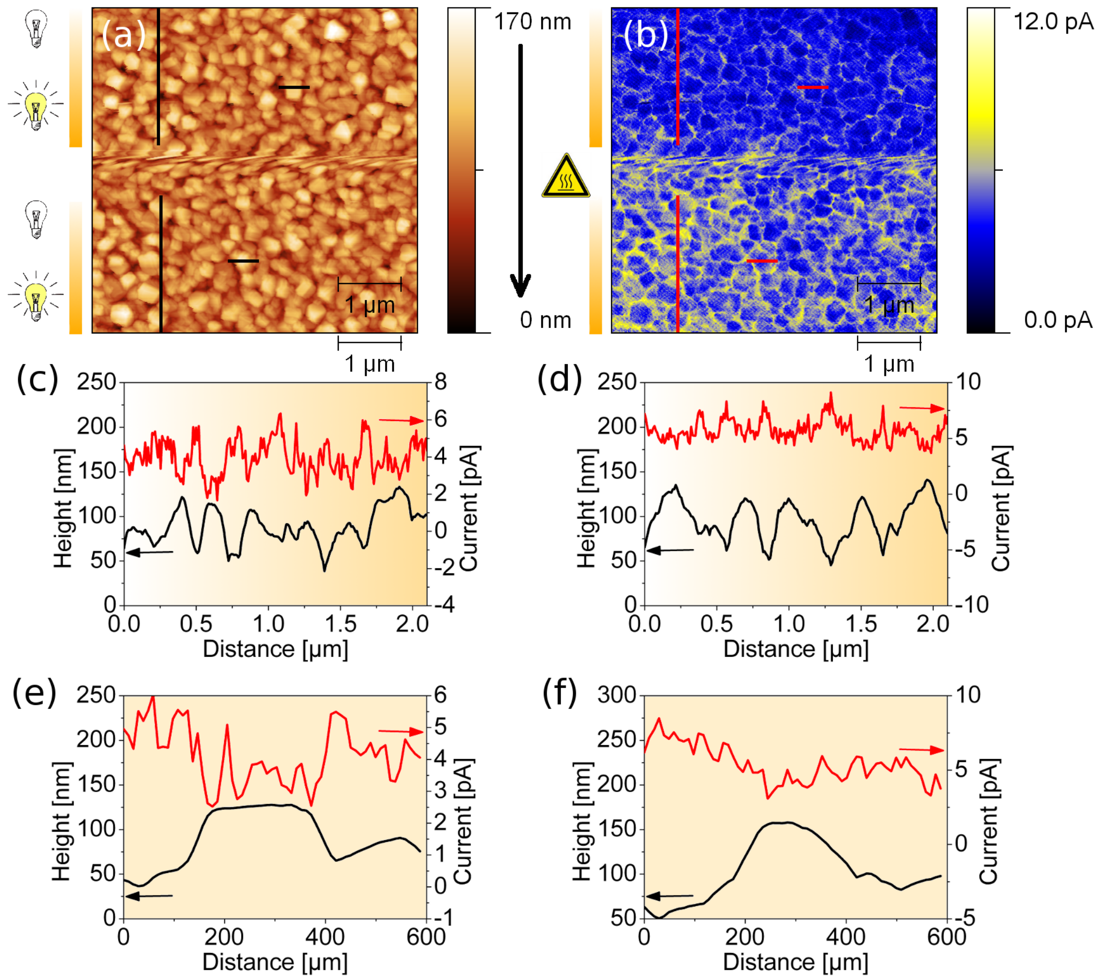

Figure 4.22: 5 μm x 5 μm PC-AFM image of a 300 nm thick partly crystalline C_{60} film under increasing intensity of illumination of the xenon lamp. In the upper part, the sample is at 85℃, in the lower part, it is heated to 95℃. Topography (a), current map recorded at -2 V sample bias (b), the corresponding cross-sections taken along the vertical marked lines at 85℃ (c) and 95℃ (d), and along the short marked lines at 85℃ (e) and 95℃ (f).

Fig.4.22.a shows the topography image revealing grains with sizes of 200 nm – 400 nm and heights of up to 100 nm. The RMS roughness is about 20 nm. The film thickness is 350 nm. Compared to the fully crystalline film, the facets of the grains are not so well defined.

The current map and the corresponding cross-sections (Fig.4.22.b – f) show an increased current at elevated temperature, but the conductivity is not influenced by the light intensity. The lower parts of the sample seem to have a higher conductivity than the grains, but the increased measured current is most likely just an artifact due to the finite tip radius. Within the valleys the tip has a higher contact area to the film and therefore a higher current is measured. On this sample, no non-conductive grains can be observed. The film seems to be more homogeneous due to the smaller grains.

The Arrhenius plot of the partly crystalline film, presented in Fig.4.23, shows the same dependence of the current density on the temperature as the crystalline film with a slightly lower current density compared to the crystalline film at the same temperatures. The slope is about -2700 K and the E_A 0.34 eV. Again, no variation of the current density due to the change of light intensity can be observed. The small differences of the average current measured at different degrees of illumination are most likely caused by the varying topography.

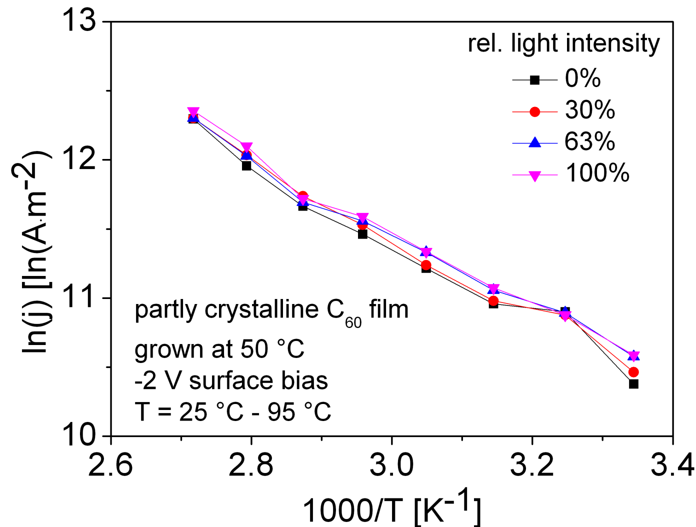

Figure 4.23: Analysis of the evaluated data of a 350 nm thick partly crystalline C_{60} film. Arrhenius plots of the current density over the inverse temperature under different degrees of illumination.

Another partly crystalline film was grown for 30 minutes with 350℃ source and 385℃ wall temperature. The substrate was cooled with the Peltier element, reaching a maximum temperature of about 50℃ during the growth process.

Fig.4.24.a shows the topography of the film, which consists of grains of about 100 nm – 500 nm in size and heights of up to 100 nm. The film has a thickness of 340 nm. Only

a few defined facets can be observed, with angles of about 120° – 140° between the facets. The RMS roughness is about 25 nm. Between the grains very high currents can be measured, which are up to 50 times higher than the currents measured in other samples at similar temperatures. This is shown in the cross-sections Fig.4.24.c – f. This phenomenon can be explained by tunneling of the current through the film. The dark lines in the current image, presented in Fig.4.24.b, at the beginning of the heating process, are due to a temporarily loss of the contact between the tip and the sample.

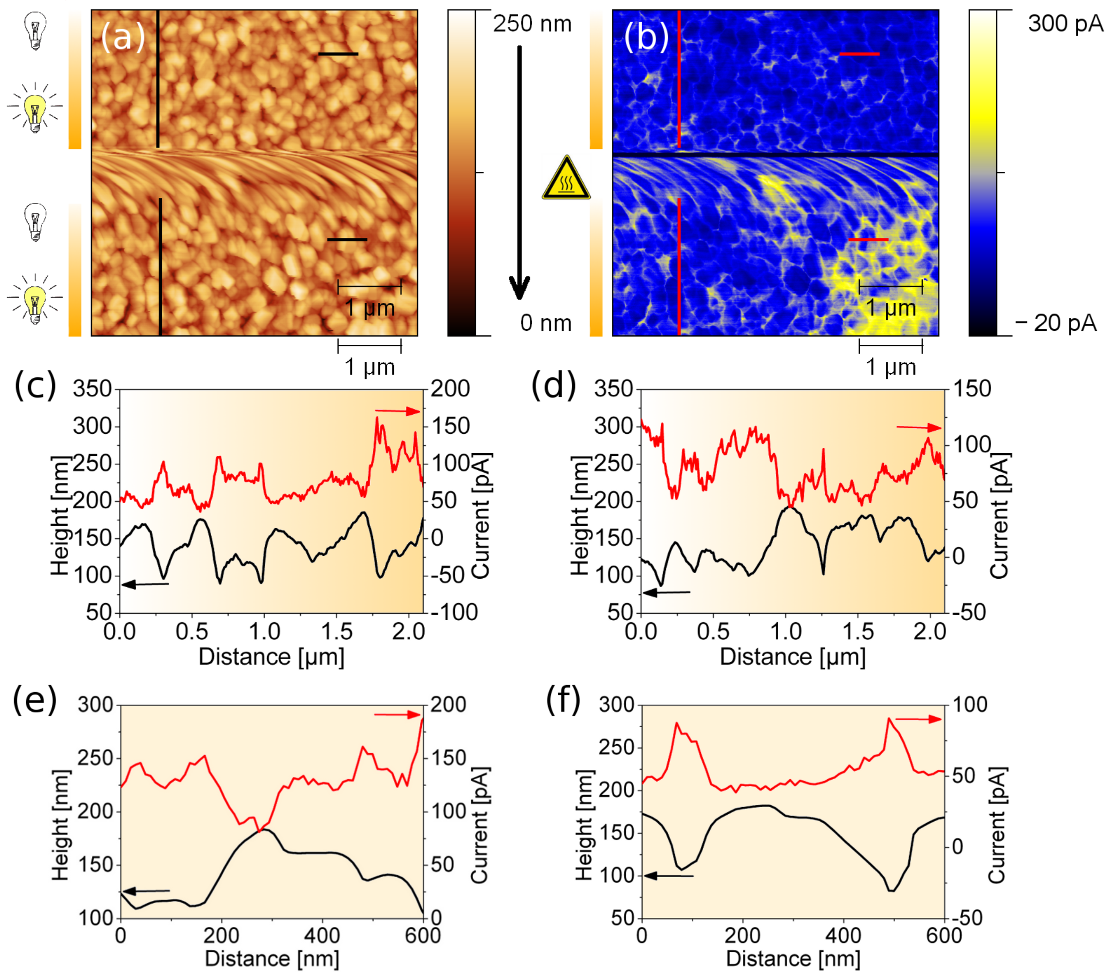

Figure 4.24: 5 μm x 5 μm PC-AFM image of a 340 nm thick partly crystalline C_{60} film under increasing intensity of illumination of the xenon lamp. In the upper part, the sample is at 70°C, in the lower part, it is heated to 80°C. Topography (a), current map recorded at -2 V sample bias (b), the corresponding cross-sections taken along the vertical marked lines at 70°C (c) and 80°C (d), and along the short marked lines at 70°C (e) and 80°C (f).

Amorphous Film

This film was grown with 350°C source and 385°C wall temperature for 45 minutes. The substrate was cooled with the Peltier element to have an almost constant temperature of about 30°C. Since the heating of the substrate through the ovens of the wall and source was too high the sample had to be taken out of the quartz tube every 15 minutes to cool down again.

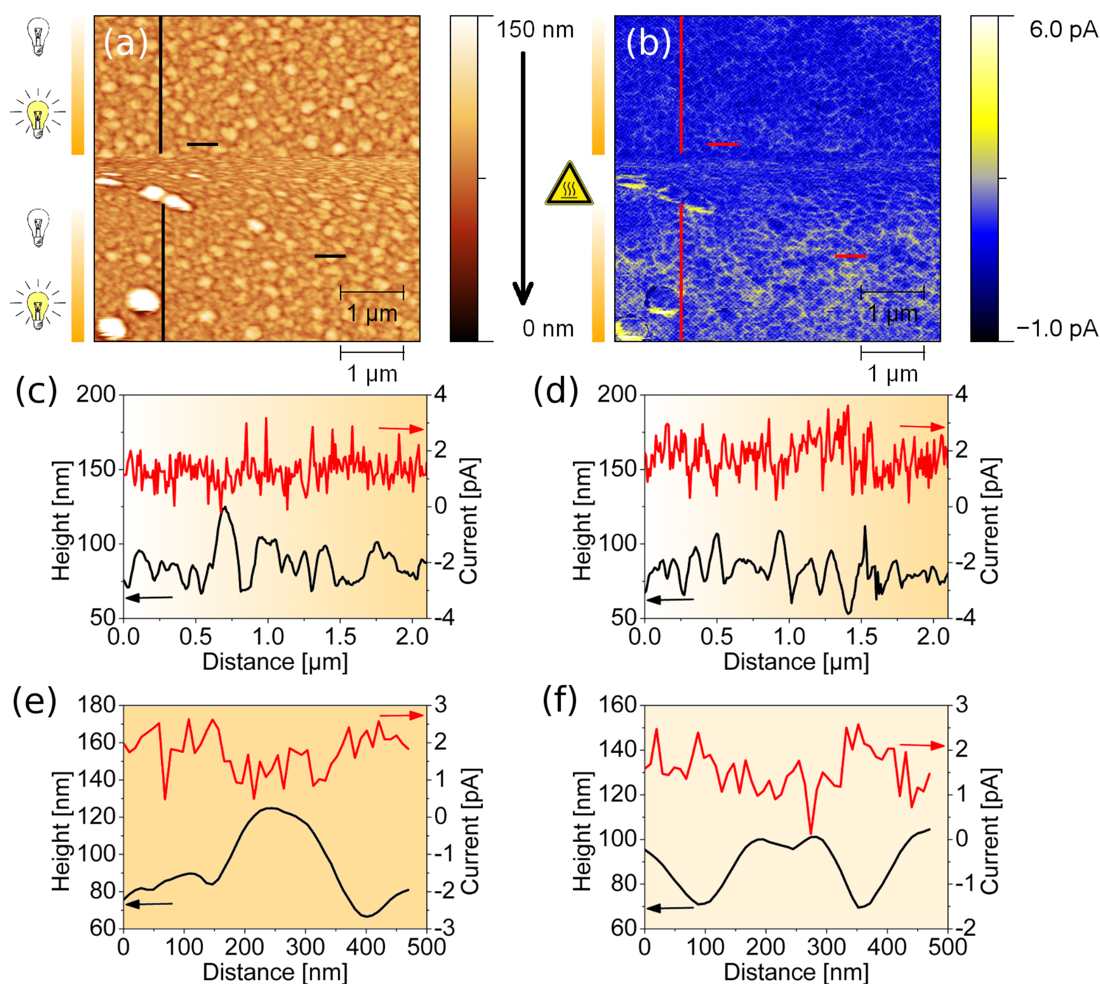

Figure 4.25: 5 μm x 5 μm PC-AFM image of a 280 nm thick amorphous C_{60} film under increasing intensity of illumination of the xenon lamp. In the upper part, the sample is at 105°C, in the lower part, it is heated to 115°C. Topography (a), current map recorded at -2 V sample bias (b), the corresponding cross-sections taken along the vertical marked lines at 105°C (c) and 115°C (d), and along the short marked lines at 105°C (e) and 115°C (f).

The topography image, presented in Fig.4.25.a, shows particles with round shape and sizes between 50 nm – 200 nm. The particles are up to 50 nm high. Some bigger

clusters can be observed with 600 nm in diameter and up to 200 nm high. The RMS roughness of the sample is about 15 nm. The film has a thickness of about 280 nm.

The current map (Fig.4.25.b) shows again an increase in current with higher temperature, but no response to light (Fig.4.25.c & d). The current in the valleys is increased, as demonstrated in the cross-sections Fig.4.25.e & f. As mentioned before this is most likely a tip artifact.

In the Arrhenius plot, shown in Fig.4.26, no intersection point of the curves under different degrees of illumination can be found. Therefore, the T_{MN} cannot be determined. On the amorphous film, a lower current density is measured compared to the crystalline and partly crystalline films at the same temperatures. Apparently, the conductivity of the film decreases when it gets more amorphous. Two different slopes can be observed. The slope at lower temperatures is about -2200 K which results in an E_A of 0.19 eV, at higher temperatures the slope increases to about -4900 K resulting in an E_A of 0.42 eV. The latter E_A is in the same range as the E_A of the crystalline film, while the E_A at lower temperatures is much lower, than of the crystalline and partly crystalline film.

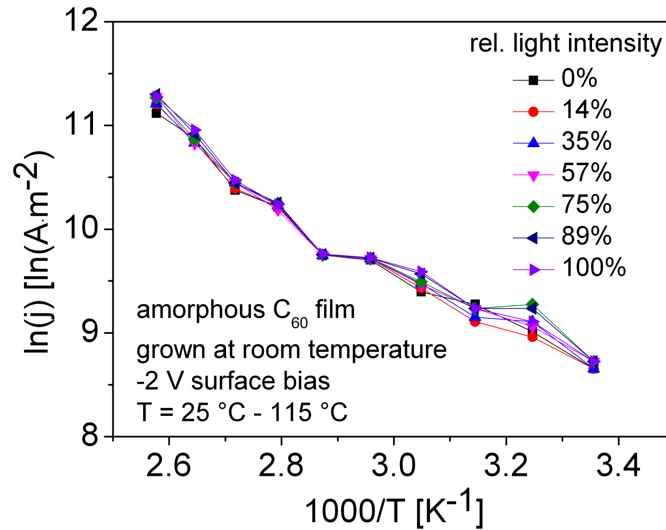

Figure 4.26: Analysis of the evaluated data of a 280 nm thick amorphous C_{60} film. Arrhenius plots of the current density over the inverse temperature under different degrees of illumination.

5 Conclusions and Outlook

In the presented work, the photoresponse in organic semiconductor thin films has been investigated utilizing PC-AFM and PA-KPFM. It could be shown that PC-AFM and PA-KPFM are appropriate tools for analyzing the photoresponse. Especially, PA-KPFM turned out to be suitable for the investigation of soft samples, which are strongly effected by the forces acting during contact mode measurements when applying PC-AFM. The samples under consideration were AnE-PV$_{stat}$: PCBM blends with varying ratios and film thicknesses, samples with PVDF-P3MT core-shell nanoparticles combined with P3HT and PCBM, as well as C_{60} thin films.

The topography images of the AnE-PV$_{stat}$: PCBM samples show particles with diameters up to 400 nm. A lower conductivity of the particles, which are expected to have a higher PCBM content – compared to the matrix – can be observed in the current images recorded by PC-AFM. The samples show a photoresponse when illuminated by an 150 W halogen lamp or an 150 W xenon lamp (white light). This was observed with PC-AFM, by an increase of the measured current under illumination, as well as with PA-KPFM by a decrease of the measured CPD. In PA-KPFM the particles have a higher CPD than the AnE-PV$_{stat}$ enriched matrix. Samples which have been in contact with air for a short time can be healed by annealing. The response to light decreases due to degradation of the sample during the measurement under ambient conditions. Rather fresh samples can be healed by annealing to 100℃ in inert atmosphere, and a photoresponse can be observed again. After longer storage of the samples in air, they cannot be healed anymore by annealing. AnE-PV$_{stat}$: PCBM blends show a clear photoresponse, but degrade in air very fast. The PCBM enriched particles have a lower conductivity compared to the AnE-PV$_{stat}$ enriched matrix.

The results of the measurements on the PVDF-P3MT/P3HT : PCBM samples are shown in Tab.5.1. The samples have been examined by means of PC-AFM and PA-KPFM. There were no signs of degradation in air over time. All samples were too soft to obtain clear images in contact mode. With KPFM a lower CPD of the particles can be observed compared to the matrix. Samples with film thicknesses below 200 nm have a smaller conductivity and show a less pronounced photoresponse. The conductivity can be increased, by adding an n-type semiconducting polymer like PCBM to the PVDF-P3MT core-shell nanoparticles with P3HT binder.

C_{60} films have been investigated by PC-AFM in order to evaluate the Meyer-Neldel rule (MNR). An Arrhenius dependence of the current density on the temperature, independent of their morphology. On neither of the samples any reaction to the change of light intensity can be observed, most likely due to very fast degradation of the sample in air. Although the films were measured in inert atmosphere, they could not be transported to nitrogen filled cell without exposure to air.

Structure	I_{dark} $[nA]$	I_{photo} $[nA]$	ΔCPD $[mV]$
PVDF-P3MT core-shell	-	-	0
PVDF-P3MT core-shell + P3HT	0.17	0.22	-
PVDF-P3MT core-shell + PCBM	-	-	0
PVDF-P3MT core-shell + P3HT + PCBM	5.20	6.30	-
P3HT + PVDF nanoparticles	-	-	0
P3HT + PCBM on PVDF	0.09	0.11	-

Table 5.1: Measurement results of the PVDF-P3MT/P3HT : PCBM samples with film thicknesses > 200 nm. I_{dark} is dark current, I_{photo} the photo current, and ΔCPD the difference in CPD without illumination and under illumination.

The Meyer-Neldel temperature (MNT) could not be determined either because of the fast degradation of the sample, or because the T_{MN} is below the available temperature range. With decreasing substrate temperature during the deposition, the film becomes amorphous. The higher conductivity is due to the better ordering in the high temperature grown sample. The lowering in the activation energy (E_A) for the more amorphous films can be attributed to the increasing density of shallow defects which makes a thermal release of charge carriers more likely.

In order to avoid damaging of the sample by the tip in contact mode, PC-AFM could also be performed in torsional resonance (TR)-mode. Here, the cantilever is oscillated in the lateral direction in a short distance from the sample, as illustrated in Fig.5.1. The tip is not in direct contact with the sample and cannot damage the surface. This method measures in the near field and a current signal can be measured from the sample to the tip via tunneling.

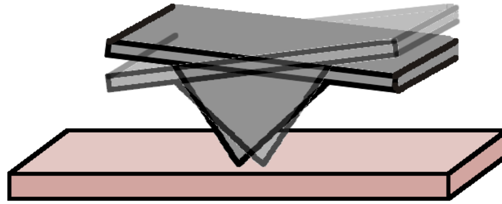

Figure 5.1: Schematic principle of torsion resonance mode.

To avoid degradation in air, PC-AFM measurements should be performed in UHV. For further improvement, the samples should even be grown in the same UHV system where the subsequent PC-AFM measurements will be performed. In this way, the samples are never exposed to air. The samples could also be grown and measured in a glove box in inert atmosphere. In this way, also measurement techniques in tapping mode, like PA-KPFM, could be performed, which are not possible in our UHV AFM systems.

Fig.5.2 shows first results of a PC-AFM measurement in UHV of an ex-situ prepared AnE-PV$_{stat}$: PCBM (1:2) blend at room temperature with -5 V applied sample bias without (Fig.5.2.a & b) and under illumination with a 532 nm laser through the window of the UHV apparatus (Fig.5.2.c & d) and the corresponding cross-sections. These measurements were performed by Stefan Lorbek and Alberto M. Ramil. A photoresponse as well as local conductivity variations can be observed. The matrix has a higher conductivity than the particles, which is consistent with the measurements performed under ambient conditions.

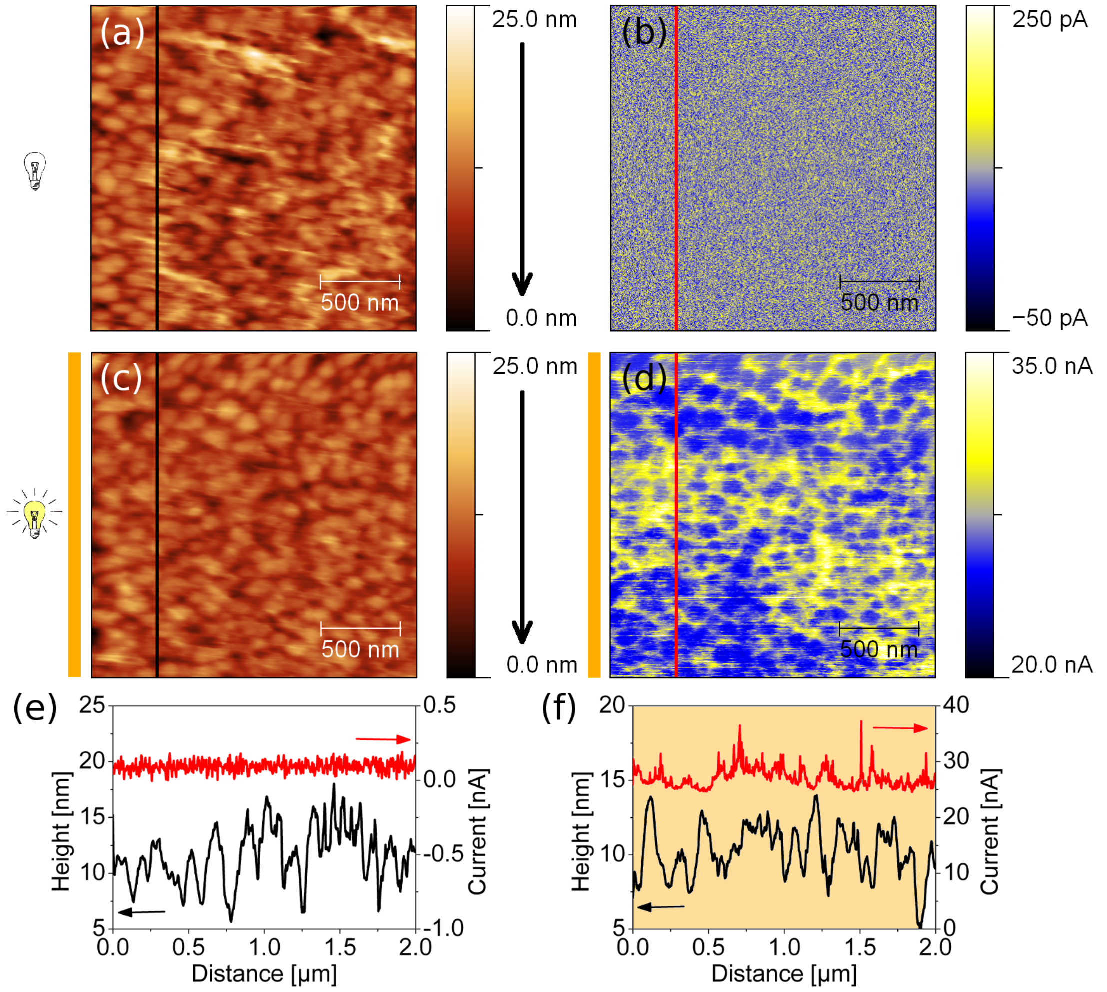

Figure 5.2: 2 μm x 2 μm PC-AFM images of an AnE-PV$_{stat}$: PCBM (1:2) blend with -5 V applied sample bias. Topography (a) and dark current map (b) as well as topography (c) and current map under illumination with a 532 nm laser (d). Corresponding cross-sections taken along the marked lines of topography and dark current image (e) and current under illumination (f).

Acknowledgments

Special thanks go to my supervisor, **Prof. Dr. Christian Teichert**, for his support and the opportunities he gave me to meet interesting colleagues in Austria and abroad.

I am thankful to my colleagues **Dr. Markus Kratzer** and **Dr. Igor Beinik** for their help in working with AFM and HWE, and nice discussions on every day problems.

I want to thank **Dr. Franz J. Schmied** for helping with software related problems, **Dipl. Ing. Stefan Lorbek** for very amusing discussions, **Dipl. Ing. Andreas Pavitschitz** for interesting chats and **Dipl. Ing. Quan Shen** for the nice time. Furthermore, I want to thank my fellow diploma students in our group **Christian Ganser** for an amusing time during the conference in Dresden, **Abdellatif Jerrar** for the shared time during work and studies, **Lin Wang** for the nice time during our measurements in Prague and **Mario Lugger** for the time shared during our studies.

I am thankful to **Prof. Ronald Meisels** for providing the current preamplifier, the Log-In amplifier and the Keithley sourcemeters, which enabled my measurements.

For their help with administrative problems, I would like to thank **Ms. Heide Kirchberger** and **Ms. Magdalena Ottrin**.

Many thanks to **Dr. Mujeeb Ullah**, **Dr. Alberto M. Ramil**, **Prof. Dr. Valery N. Bliznyuk**, **Prof. Dr. Helmut Sitter**, **Prof. Dr. Niyazi S. Sariciftci** from the JKU Linz for providing samples, the joint measurements, and interesting discussions.

I would like to thank all friends for the great time in Leoben and the many experiences we have shared. I am also grateful to my former teachers **Mag. Ursula Patzer** and **Mag. Anna Döller-Gundacker** for their support on everyday problems in the past, **Dr. Werner Soukup** and **Mag. Johann Ganzberger** for supporting my interests in physics and chemistry and encouraging me in choosing this study, and **Mag. Johann Wenzel** and **Mag. Brigitte Fiska** for teaching me English in an interesting way.

Most of all I want to thank my parents for their great support during all the time and my brother for his encouragements.

Furthermore, I want to thank the Austrian Science Fund (**FWF - NFN**) for financial support within the project "Interface controlled and fictionalized organic thin films", project number S9707-N20.

List of Figures

2.1 Chemical structures of the studied polymers: all types of AnE-PV and the different side chains octyl and 2-ethylhexyl [16] (a), P3HT [11] (b), PVDF (c), PCBM [11] (d) and P3MT [17] (e). 6
2.2 Macroscopic measurements of the field effect charge carrier mobility in a C_{60} OFET as function on temperature and charge carrier concentration modified via the applied gate voltage V_G (red points). The isokinetic temperature T_{MN}, here T_0, is indicated by an arrow. The C_{60} film was grown via hot wall epitaxy at 250°C substrate temperature. (From [20].) 7
2.3 Schematic drawing of a HWE-setup. 9
2.4 Schematic setup of a PC-AFM measurement. To avoid confusion, the feedback laser and diodes of the AFM are not shown. For illumination from the top, special probe geometries have to be used. 11
2.5 Schematic setup of a KPFM measurement. During the first scan of the line the topography image is recorded, during the second scan the tip stays in a constant distance to the previously measured surface, and the CPD is measured. 12

3.1 The vacuum chamber of the HWE with Peltier element, Quartz tube, and Substrate holder (a). The complete setup including vacuum pumps and electronics (b). 14
3.2 Asylum Research MFP-3D™ system at the Institute of Physics in Leoben. Right to the AFM from bottom to top are a Lock-In Amplifier from Stanford Research Systems, an external current preamplifier from DL Instruments and two Keithley 2400 sourcemeters to apply higher sample bias than the MFP can apply. 15
3.3 Emission spectra of the light sources used for illumination: From the bulb lamp of the optical microscope of the MFP-3D™ (a) and the xenon lamp (b). 16
3.4 SEM image of an AdvancedTEC™ probe from NANOSENSORS™ applicable for PC-AFM and PA-KPFM with illumination from the top. (From [29]) 17
3.5 A schematic drawing of the polymer heater (from [30]) (a), and an assembled setup with a C_{60} sample and the necessary wiring (b). Additionally, the tube for the nitrogen has to be plugged into the vacant notch. . . . 18

4.1 5 μm x 5 μm PC-AFM image of a 210 nm thick AnE-PV$_{stat}$: PCBM (1:2) blend partly illuminated with the bulb lamp, indicated by the orange bars left to the images, measured at room temperature. The scanning direction is from the top to the bottom of the image, indicated by an arrow. Topography (a), current map recorded at -2 V sample bias (b) and the corresponding cross-sections taken along the vertical marked line in scanning direction (c). 20
4.2 2 μm x 2 μm PC-AFM image of a 200 nm thick AnE-PV$_{stat}$: PCBM (1:2) blend partly illuminated with the bulb lamp measured at room temperature. Topography (a), current map recorded at -2 V sample bias (b), the corresponding cross-sections taken along the vertical marked line in scanning direction (c), and along the short marked line of a less conductive particle under illumination (d). A degradation of the sample during the scanning can be observed in the current map. 21
4.3 I-V curves measured on an arbitrary point on a AnE-PV$_{stat}$: PCBM (1:2) blend under illumination (orange curve) and non illuminated (black curve). At room temperature (a) and at 100℃ (b). 22
4.4 2 μm x 2 μm PC-AFM image of a 170 nm thick AnE-PV$_{stat}$: PCBM (1:3) blend partly illuminated by a LED with 490 nm wavelength measured at room temperature. Topography (a), current map recorded at -3 V sample bias (b), the corresponding cross-sections taken along the vertical marked line in scanning direction (c), and along the short marked line of a less conductive particle without illumination (d). 23
4.5 10 μm PA-KPFM measurement of a 260 nm thick AnE-PV$_{stat}$: PCBM (1:1) blend partly illuminated with the bulb lamp measured at 100℃. The scan started at the top. The slow scan axis was disabled, whereby only one scan line was scanned over the whole image. Topography (a), contact potential difference map (b), the corresponding cross-sections taken along the marked lines without illumination (c), and under illumination (d). 24
4.6 25 μm x 25 μm PA-KPFM image of a 260 nm AnE-PV$_{stat}$: PCBM (1:1) blend illuminated with the bulb lamp measured at 100℃. In the upper part of the image the slow scan axis was disabled. Topography (a), contact potential difference map (b), and the corresponding cross-sections taken along the vertical marked line in scanning direction (c). . 25
4.7 2 μm x 2 μm PC-AFM image of a 90 nm thick AnE-PV$_{stat}$: PCBM (1:3) blend partly illuminated with the xenon lamp measured at room temperature. Topography (a), current map recorded at +1 V sample bias (b), the corresponding cross-sections taken along the vertical marked line in scanning direction (c), I-V curves under illumination (orange), and non illuminated (black) recorded on the matrix (d). In the lower left corner a contamination is visible in the topography and the current map. 26

4.8 2 μm x 2 μm PC-AFM image of a 90 nm AnE-PV$_{stat}$: PCBM (1:3) blend partly illuminated with the xenon lamp measured at 100°C. Topography (a), current map recorded at +1 V sample bias (b), the corresponding cross-sections taken along the vertical marked line in scanning direction (c), and along the short marked line of a less conductive particle without illumination (d), as well as I-V curves under illumination (orange) and unilluminated (black) recorded on the matrix (e). 27
4.9 1 μm x 1 μm PC-AFM image of a 60 nm thick AnE-PV$_{stat}$: PCBM (1:1) blend partly illuminated with the xenon lamp and measured at room temperature. Topography (a), current map recorded at -1 V sample bias (b), and the corresponding cross-sections taken along the vertical marked line in scanning direction (c). 28
4.10 5 μm x 5 μm PA-KPFM image of a 60 nm AnE-PV$_{stat}$: PCBM (1:1) blend partly illuminated with the xenon lamp, measured at room temperature after annealing to 100°C. Topography (a), contact potential difference map(b), the corresponding cross-sections taken along the vertical marked line in scanning direction (c), and along the short marked line of a less conductive particle under illumination (d). 29
4.11 2 μm x 2 μm PC-AFM image of PVFD-P3MT core-shell nanoparticles with P3HT binder partly illuminated with the bulb lamp measured at room temperature. The film thickness is 260 nm. Topography (a), current map recorded at +2 V sample bias (b), and the corresponding cross-sections taken along the vertical marked line in scanning direction (c). 30
4.12 2 μm x 2 μm PC-AFM image of PVFD-P3MT core-shell nanoparticles with P3HT binder on PEDOT partly illuminated with the bulb lamp and measured at room temperature. The film thickness is 260 nm. Topography (a), current map recorded at -2 V sample bias (b), and the corresponding cross-sections taken along the vertical marked line in scanning direction (c). 31
4.13 2 μm x 2 μm PC-AFM image of PVFD-P3MT core-shell nanoparticles with P3HT binder on PEDOT partly illuminated with the bulb lamp and measured at room temperature. The film thickness is 170 nm. Topography (a), current map recorded at +10 V sample bias (b), and the corresponding cross-sections taken along the vertical marked line in scanning direction (c). 32
4.14 2 μm x 2 μm PC-AFM image of PVFD-P3MT core-shell nanoparticles with P3HT binder and PCBM drop cast on PEDOT partly illuminated with the bulb lamp and measured at room temperature. The film thickness is 200 nm. Topography (a), current map recorded at -2 V sample bias (b) and the corresponding cross-sections taken along the vertical marked line in scanning direction (c), and along the short marked line of a less conductive particle under illumination (d). 33

4.15 2 μm x 2 μm PC-AFM image of an P3HT : PCBM (1:1) blend on PVDF partly illuminated with the bulb lamp and measured at room temperature. The film thickness is 250 nm. Topography (a), current map recorded at +2 V sample bias (b), and the corresponding cross-sections taken along the marked line in scanning direction (c). 34
4.16 5 μm x 5 μm PA-KPFM image of PVDF-P3MT core-shell nanoparticles partly illuminated with the bulb lamp and measured at room temperature. The film thickness is 1.3 μm. Topography (a), contact potential difference map (b), and the corresponding cross-sections taken along the vertical marked line in scanning direction (c). 35
4.17 5 μm x 5 μm PA-KPFM image of a PVDF-P3MT core-shell nanoparticles : PCBM (2:1) blend partly illuminated with the bulb lamp and measured at room temperature. The film thickness is 2 μm. Topography (a), contact potential difference map (b), and the corresponding cross-sections taken along the vertical marked line in scanning direction (c). 36
4.18 5 μm x 5 μm PA-KPFM image of P3HT with PVDF nanoparticles partly illuminated with the bulb lamp and measured at room temperature. The average film thickness is 300 nm. Topography (a), contact potential difference map (b), the corresponding cross-sections taken along the vertical marked line in scanning direction (c), and along the short marked line of a cluster with lower CPD without illumination (d). 37
4.19 Setup of the measurements on C_{60} thin films with ATEC-Cont probes, the external preamplifier, the xenon lamp, and an adjustable slit. . . . 38
4.20 5 μm x 5 μm PC-AFM image of a 800 nm thick crystalline C_{60} film under increasing intensity of illumination of the xenon lamp. In the upper part, the sample is at 100℃, in the lower part at 110℃. Topography (a), current map recorded at -2 V sample bias (b), the corresponding cross-sections taken along the vertical marked lines at 100℃ (c) and 110℃ (d), and the cross-sections of single non-conductive grains taken along the short marked lines at 100℃ (e) and at 110℃ (f). 39
4.21 Analysis of the evaluated data of a crystalline 800 nm thick C_{60} film. Arrhenius plots of the current density over the inverse temperature under different degrees of illumination. 40
4.22 5 μm x 5 μm PC-AFM image of a 300 nm thick partly crystalline C_{60} film under increasing intensity of illumination of the xenon lamp. In the upper part, the sample is at 85℃, in the lower part, it is heated to 95℃. Topography (a), current map recorded at -2 V sample bias (b), the corresponding cross-sections taken along the vertical marked lines at 85℃ (c) and 95℃ (d), and along the short marked lines at 85℃ (e) and 95℃ (f). 41
4.23 Analysis of the evaluated data of a 350 nm thick partly crystalline C_{60} film. Arrhenius plots of the current density over the inverse temperature under different degrees of illumination. 42

4.24 5 μm x 5 μm PC-AFM image of a 340 nm thick partly crystalline C_{60} film under increasing intensity of illumination of the xenon lamp. In the upper part, the sample is at 70℃, in the lower part, it is heated to 80℃. Topography (a), current map recorded at -2 V sample bias (b), the corresponding cross-sections taken along the vertical marked lines at 70℃ (c) and 80℃ (d), and along the short marked lines at 70℃ (e) and 80℃ (f). 43
4.25 5 μm x 5 μm PC-AFM image of a 280 nm thick amorphous C_{60} film under increasing intensity of illumination of the xenon lamp. In the upper part, the sample is at 105℃, in the lower part, it is heated to 115℃. Topography (a), current map recorded at -2 V sample bias (b), the corresponding cross-sections taken along the vertical marked lines at 105℃ (c) and 115℃ (d), and along the short marked lines at 105℃ (e) and 115℃ (f). 44
4.26 Analysis of the evaluated data of a 280 nm thick amorphous C_{60} film. Arrhenius plots of the current density over the inverse temperature under different degrees of illumination. 45

5.1 Schematic principle of torsion resonance mode. 47
5.2 2 μm x 2 μm PC-AFM images of an AnE-PV$_{stat}$: PCBM (1:2) blend with -5 V applied sample bias. Topography (a) and dark current map (b) as well as topography (c) and current map under illumination with a 532 nm laser (d). Corresponding cross-sections taken along the marked lines of topography and dark current image (e) and current under illumination (f). 48

Bibliography

[1] H. Hoppe and N.S. Sariciftci. Organic solar cells: An overview. *Journal of Materials Research*, 19:1925, 2004.

[2] V.L. Mironov. Fundamentals of the scanning probe microscopy. *Journal of Nanoscience and Nanotechnology*, 4:647, 2004.

[3] C. Teichert and I. Beinik. *in Conductive Atomic-Force Microscopy Investigation of Nanostructures in Microelectronics*. Springer, 2011.

[4] M. Nonnenmacher, M.P. Oboyle, and H.K. Wickramasinghe. Kelvin probe force microscopy. *Applied Physics Letters*, 58:2921, 1991.

[5] I. Beinik. *Electrical Properties of Semiconductor Nanostructures by Conductive Probe Based Atomic Force Microscopy*. PhD Thesis, Montanuniversität Leoben, 2011.

[6] M. Schwoerer and H.C. Wolf. *Organic molecular solids*. Wiley-VCH, Weinheim, 2007.

[7] A. Goetzberger and V.U. Hoffmann. *Photovoltaic solar energy generation*. Springer Verlag, 2005.

[8] N.S. Sariciftci, L. Smilowitz, A.J. Heeger, and F. Wudl. Photoinduced electron transfer from a conducting polymer to buckminsterfullerene. *Science*, 258:1474, 1992.

[9] L. Smilowitz, NS Sariciftci, R. Wu, C. Gettinger, A.J. Heeger, and F. Wudl. Photoexcitation spectroscopy of conducting-polymer–C_{60} composites: Photoinduced electron transfer. *Physical Review B*, 47:13835, 1993.

[10] L.E. Greene, M. Law, B.D. Yuhas, and P. Yang. ZnO-TiO2 core-shell nanorod/P3HT solar cells. *The Journal of Physical Chemistry C*, 111:18451, 2007.

[11] G. Weihao. An overview on P3HT:PCBM, the most efficient organic solar cell material so far. *Solid State Physics II Journal*, 2009.

[12] D.A.M. Egbe, G. Adam, A. Pivrikas, A.M. Ramil, E. Birckner, V. Cimrova, H. Hoppe, and N.S. Sariciftci. Improvement in carrier mobility and photovoltaic performance through random distribution of segments of linear and branched side chains. *Journal of Materials Chemistry*, 20:9726, 2010.

[13] H. Kawai. The piezoelectricity of PVDF. *Japanese Journal of Applied Physics*, 8:975, 1969.

[14] Y. Bormashenko, R. Pogreb, O. Stanevsky, and E. Bormashenko. Vibrational spectrum of PVDF and its interpretation. *Polymer testing*, 23:791, 2004.

[15] F.C. Krebs. Fabrication and processing of polymer solar cells: a review of printing and coating techniques. *Solar Energy Materials and Solar Cells*, 93:394, 2009.

[16] D.A.M. Egbe, S. Türk, S. Rathgeber, F. Kühnlenz, R. Jadhav, A. Wild, E. Birckner, G. Adam, A. Pivrikas, V. Cimrova, G. Knör, N.S. Sariciftci, and H. Hoppe. Anthracene Based Conjugated Polymers: Correlation between π-π-Stacking Ability, Photophysical Properties, Charge Carrier Mobility, and Photovoltaic Performance. *Macromolecules*, 43:1261, 2010.

[17] S. Tagmouti, A. Outzourhit, A. Oueriagli, M. Khaidar, M. Elyacoubi, R. Evrard, and EL Ameziane. Electrical characteristics of W/P3MT/Pt diodes. *Thin Solid Films*, 379:272, 2000.

[18] W. Meyer and H. Neldel. Beziehungen zwischen der Energiekonstanten ε und der Mengenkonstanten a in der Leitwerts-Temperaturformel bei oxydischen Halbleitern. *Zeitschrift für technische Physik*, 12:588, 1937.

[19] P. Stallinga and H.L. Gomes. Explanation of the Meyer-Neldel Rule. *Energy*, 8:13, 2005.

[20] M. Ullah, I.I. Fishchuk, A. Kadashchuk, P. Stadler, A. Pivrikas, C. Simbrunner, V.N. Poroshin, N.S. Sariciftci, and H. Sitter. Dependence of Meyer–Neldel energy on energetic disorder in organic field effect transistors. *Applied Physics Letters*, 96:213306, 2010.

[21] E.J. Meijer, M. Matters, P.T. Herwig, D.M. de Leeuw, and T.M. Klapwijk. The Meyer–Neldel rule in organic thin-film transistors. *Applied Physics Letters*, 76:3433, 2000.

[22] H. Sitter, A. Andreev, G. Matt, and N.S. Sariciftci. Hot wall epitaxial growth of highly ordered organic epilayers. *Synthetic Metals*, 138:9, 2003.

[23] G. Matt. *Fullerene-Oligophenyl multilayers grown by hot wall epitaxy*. Masterthesis, Johannes Kepler University Linz, 1999.

[24] T.R. Thomas. *Rough surfaces*. Imperial College Press London, 1999.

[25] R. Giridharagopal, G. Shao, C. Groves, and D.S. Ginger. New SPM techniques for analyzing OPV materials. *Materials Today*, 13:50, 2010.

[26] P.P. Craig and V. Radeka. Stress dependence of contact potential: The AC Kelvin method. *Review of Scientific Instruments*, 41:258, 1970.

[27] G. Ertl, J. Küppers, and M. Grasserbauer. *Low energy electrons and surface chemistry*. Verlag Chemie, 1985.

[28] S. Sadewasser, T. Glatzel, R. Shikler, Y. Rosenwaks, and M.C. Lux-Steiner. Resolution of Kelvin probe force microscopy in ultrahigh vacuum: comparison of experiment and simulation. *Applied Surface Science*, 210:32, 2003.

[29] http://www.nanosensors.com/AdvancedTEC.pdf.

[30] http://www.asylumresearch.com/Products/PolyHeater/PolyHeater.shtml.

[31] D. Sarid. *Exploring scanning probe microscopy with Mathematica*. Wiley-VCH, Weinheim, 2007.

[32] H. Coufal, K. Meyer, R.K. Grygier, M. Vries, D. Jenrich, and P. Hess. Measurement of the elastic properties of evaporated C_{60} films by surface acoustic waves. *Applied Physics A: Materials Science & Processing*, 59:83, 1994.

[33] A.F. Hebard, R.C. Haddon, R.M. Fleming, and A.R. Kortan. Deposition and characterization of fullerene films. *Applied Physics Letters*, 59:2109, 1991.

[34] W.M. Tong, D.A.A. Ohlberg, H.K. You, R.S. Williams, S.J. Anz, M.M. Alvarez, R.L. Whetten, Y. Rubin, and F.N. Diederich. X-ray diffraction and electron spectroscopy of epitaxial molecular buckminsterfullerene films. *The Journal of Physical Chemistry*, 95:4709, 1991.